

Activation of *Shaker* Potassium Channels

I. Characterization of Voltage-dependent Transitions

N.E. SCHOPPA and F.J. SIGWORTH

From the Department of Cellular and Molecular Physiology, Yale University School of Medicine, New Haven, Connecticut 06520

ABSTRACT The conformational changes associated with activation gating in *Shaker* potassium channels are functionally characterized in patch-clamp recordings made from *Xenopus laevis* oocytes expressing *Shaker* channels with fast inactivation removed. Estimates of the forward and backward rates for transitions are obtained by fitting exponentials to macroscopic ionic and gating current relaxations at voltage extremes, where we assume that transitions are unidirectional. The assignment of different rates is facilitated by using voltage protocols that incorporate prepulses to preload channels into different distributions of states, yielding test currents that reflect different subsets of transitions. These data yield direct estimates of the rate constants and partial charges associated with three forward and three backward transitions, as well as estimates of the partial charges associated with other transitions. The partial charges correspond to an average charge movement of $0.5 e_0$ during each transition in the activation process. This value implies that activation gating involves a large number of transitions to account for the total gating charge displacement of $13 e_0$. The characterization of the gating transitions here forms the basis for constraining a detailed gating model to be described in a subsequent paper of this series.

KEY WORDS: ion channel • gating current • single-channel current • patch clamp • kinetic model

INTRODUCTION

Voltage-gated sodium, calcium, and potassium channels underlie the electrical properties of excitable cells. Insights into the structural changes involved in the voltage-dependent opening of these channels first came from functional studies performed in the squid axon (Hodgkin and Huxley, 1952*a*, 1952*b*). The steep voltage sensitivity of the observed potassium and sodium conductances suggested that the channel opening process involves the displacement of a large amount of charge across the cell membrane. The long delay in the time courses of activation implied that channel opening involves multiple kinetic steps. The structural origins of these functional properties are now becoming clear. The alpha subunits of voltage-gated sodium and calcium channels are each encoded by a single long transcript with four homologous regions (Noda et al., 1984; Tanabe et al., 1987), while voltage-gated potassium channels are encoded by a transcript that is approximately one-fourth as long (Tempel et al., 1987; Kamb et al., 1988), with a channel complex formed by four subunits (MacKinnon, 1991; Kavanaugh et al.,

1992; Li et al., 1994). A requirement for separate activation of each of these units helps to explain the delay in channel activation. Each of the protomers or subunits of these channels contains a putative transmembrane segment S4 that has a number of conserved basic residues and is a candidate for the charged region of the channel that moves in response to voltage, leading to channel activation (Guy and Seetharamulu, 1986; Noda et al., 1986). Mutations in the S4 region yield large effects on the voltage dependence of activation (Stühmer et al., 1989; Liman et al., 1991; Lopez et al., 1991; McCormack et al., 1991; Papazian et al., 1991; Logothetis et al., 1992; summarized in Sigworth, 1994). Also, it has been shown recently that membrane potential changes cause changes in accessibility of S4 residues (Yang and Horn, 1995; Yang et al., 1996; Mannuzzu et al., 1996; Larsson et al., 1996), and that S4 charge changes cause changes in total gating charge movement (Aggarwal and MacKinnon, 1996; Seoh et al., 1996).

Insights into the mechanics of activation gating have also come from extensions of the functional studies that were first performed by Hodgkin and Huxley (1952*a*, 1952*b*). In voltage-clamp measurements of macroscopic and single-channel ionic currents, various voltage protocols have been used to emphasize particular steps in the activation process (Cole and Moore, 1960). The voltage-dependent transitions among closed states have also been characterized from the time courses of gating currents, which are the direct electrical manifestation of the charge displacements as-

Dr. Schoppa's present address is Vollum Institute, Oregon Health Sciences University L-474, Portland, OR 97201-3098.

Address correspondence to Fred J. Sigworth, Department of Cellular and Molecular Physiology, Yale University School of Medicine, 333 Cedar Street, New Haven, CT 06520. Fax: 203-785-4951; E-mail: fred.sigworth@yale.edu

sociated with conformational changes (Armstrong and Bezanilla, 1973; Schneider and Chandler, 1973; Keynes and Rojas, 1974). Additionally, the fluctuations in the gating currents can provide information about the size of the charge displacements in single gating transitions (Conti and Stühmer, 1989; Crouzy and Sigworth, 1993; Sigg et al., 1994b). Ultimately, the understanding of voltage gating in ion channels will require combining this detailed functional information with experiments that give more direct structural information.

Examples of the value of detailed functional studies are seen in the recent work on the *Shaker* potassium channel (Bezanilla et al., 1991; Stühmer et al., 1991; Schoppa et al., 1992; Bezanilla et al., 1994; Hoshi et al., 1994; McCormack et al., 1994; Perozo et al., 1994; Stefani et al., 1994; Zagotta et al., 1994a, 1994b). *Shaker* channels have been a favorite in the study of activation gating for a variety of reasons. They can be made non-inactivating through a NH₂-terminal truncation (Hoshi et al., 1990) and they express well in *Xenopus* oocytes, allowing the measurement of gating currents as well as ionic currents. Also, because they are tetramers, the presumed fourfold functional symmetry of *Shaker* channels can be exploited in developing simpler kinetic models. The major results from the recent studies on these channels may be summarized as follows.

(a) The total gating charge per channel is $\sim 13 e_0$. This value was obtained from calibrated measurements of gating currents (Schoppa et al., 1992; Aggarwal and MacKinnon, 1996; Seoh et al., 1996), and corroborated by measurements of limiting voltage sensitivity (Zagotta et al., 1994a; Seoh et al., 1996).

(b) Between the resting and the open state, the channel undergoes a minimum of five kinetic transitions, as estimated from the time course of channel opening in response to a voltage step (Zagotta et al., 1994a).

(c) The time course of the "on" gating current induced by a step depolarization has a rising or plateau phase (Bezanilla et al., 1994), implying that the first kinetic steps in channel activation are slower or less voltage dependent than subsequent steps.

(d) After large depolarizations, the time course of the "off" gating current induced by a voltage step back to the holding potential has a rising phase (Bezanilla et al., 1991) and also decay kinetics that match the time course of channel deactivation (Zagotta et al., 1994a). Thus, the first kinetic steps in channel deactivation are slower than subsequent steps.

(e) At intermediate voltages, the gating currents display a fast component that is followed by a slow exponential component that is correlated with channel opening (Bezanilla et al., 1994). Also, at these voltages, the ionic currents have a relatively short delay, followed by a very slow rise to the peak current (Zagotta et al., 1994a). These phenomena imply that channel opening

at these voltages is much slower than the rate that the channel traverses through early closed states.

(f) *Shaker's* voltage dependence of charge movement (Q - V) relation is shallow at hyperpolarized voltages but is steeper over the voltage range where channels open (Stefani et al., 1994; Bezanilla et al., 1994).

(g) Components of charge in the Q - V relation have been shown to be differentially affected by some mutations in the S4 region (Schoppa et al., 1992; Perozo et al., 1994) and also by drug binding (McCormack et al., 1994). The differential effects suggest the existence of different types of voltage-dependent conformational changes.

(h) Measurements of gating current fluctuations suggest that elementary charge movements are roughly 2 e_0 in size (Sigg et al., 1994b; Sigworth, 1994).

(i) The distribution of channel open times is well described by a single exponential function (Hoshi et al., 1994), which is consistent with *Shaker* channels having a single open state. The single channel data also suggest the presence of closed states that are not in the main activation path (Hoshi et al., 1994).

Several kinetic models have been proposed that take into account subsets of these functional properties for *Shaker* channels (Schoppa et al., 1992; Tytgat and Hess, 1992; Bezanilla et al., 1994; McCormack et al., 1994; Zagotta et al., 1994b). Interestingly, however, these models have little in common with each other, with different models explaining the same functional data through very different mechanisms. For example, the steep voltage dependence of charge movement and channel opening is explained in the model proposed by Bezanilla et al. (1994) by a transition with a large valence, while the model of Zagotta et al. (1994b) achieves this through smaller charge movements but with a slow channel closing rate. The discrepancies between the models point to the need of further analysis of the activation properties of *Shaker* channels.

In this paper and the two papers that follow (Schoppa and Sigworth, 1998a, 1998b), we present further functional studies on activation gating in *Shaker* potassium channels. Our general strategy is to perform a systematic study of the different gating steps in *Shaker's* activation process. This first paper will focus on measurements of macroscopic ionic and gating currents measured at extreme depolarizations and hyperpolarizations, which yield estimates of forward and backward rates. Some of the described experiments are similar to those that have been reported previously, but new insights into the activation gating process are gained by analyzing the data in new ways, and also by extending the voltage range of the current measurements. The channel studied, which has its NH₂ terminus truncated to remove fast inactivation, will be referred to as wild type (WT)¹ to distinguish it from a mu-

tant channel (V2) that will be the focus of the second paper. The third paper will use results from both WT and V2 channels to develop a new kinetic model for *Shaker* channel activation.

METHODS

Channel Expression

The construction of noninactivating WT *Shaker* 29-4 cDNAs and in vitro synthesis of cRNA have been described previously (Iverson et al., 1990; Schoppa et al., 1992). Channels were expressed in *Xenopus laevis* oocytes injected with ~3 ng cRNA for recordings of macroscopic ionic and gating currents, and 50–100-fold less cRNA for single channel recordings. Current measurements were made 4–21 d after injection with the patch-clamp technique (Hamill et al., 1981) using an EPC-9 patch clamp amplifier (HEKA Electronic, Lambrecht, Germany).

Measurements of Macroscopic Ionic and Gating Currents

Macroscopic ionic and gating currents were recorded in inside-out membrane patches using conventional oocyte macropatch techniques (Stühmer et al., 1991). Patch recordings used pipettes pulled from Kimax capillary tubes with tip diameters ranging from 3 to 10 μm (0.5–3.0 M Ω resistance). Voltage pulses were applied from a holding potential of -93 mV. Current signals were filtered (unless otherwise indicated) at 10 and 5 kHz (Bessel characteristic) for recordings of ionic and gating currents, respectively. Data were sampled at five to seven times the filtering frequency. For subtraction of linear leak and capacitive currents in recordings of macroscopic ionic currents, alternating positive and negative pulses of 20-mV amplitude from a -133 -mV leak holding potential were applied, and the resulting current was scaled appropriately. For gating currents, a scaled current response induced by only a negative going voltage pulse from -133 to -153 was subtracted. This modification reduced the artifact in leak subtraction from charge movement at voltages positive to -133 mV (Stühmer et al., 1991). To increase the signal-to-noise ratio, 10–100 sweeps were averaged before the data were stored. The pulse frequency was set to be high (1–5 Hz) to allow rapid measurement of many sweeps, but we determined that the frequencies used did not induce rundown of the ionic or gating currents, arising from slow inactivation. Displayed gating current traces were sometimes additionally filtered with a Gaussian digital filter to 2.5–3.5 kHz.

Most of the ionic current measurements were made with pipettes filled with 140 mM *N*-methyl-D-glucamine (NMDG) aspartate (Asp), 1.8 mM CaCl_2 , and 10 mM HEPES, and the bath solution contained 139 mM KAsp, 1 mM KCl, 1 mM EGTA, and 10 mM HEPES. Most of the gating current measurements were made with the same solutions, except with 2 μM charybdotoxin (CTx) added to the pipette solution to block ionic currents (Lucchesi et al., 1989). CTx did not appear to alter the properties of the charge movement, as the currents recorded in the presence of CTx were similar to those recorded in the absence of CTx but with NMDG⁺ replacing K⁺ in the bath to remove the ionic current. Membrane potential values were corrected for a liquid junction potential at the interface of the NMDG⁺ pipette and K⁺ bath

solutions, which we estimated to be -13 mV (Neher, 1992). All experiments were done at room temperature. The bath chamber was not perfused in these experiments.

Voltage steps to very positive and negative voltages were kept short (≤ 5 ms at $V > +100$ mV and $V < -120$ mV) to reduce contamination of the recorded ionic currents by endogenous oocyte currents. Corresponding gating current recordings made in the presence of CTx showed little background current, suggesting that contamination of our ionic currents by endogenous currents is likely to be negligible.

The large pipette sizes used in recordings of gating currents encouraged the formation of membrane vesicles or partial vesicles when the patch was pulled off the oocyte. Gating current recordings were rejected if the measured on current did not show an instantaneous component of the rising phase: specifically, a component with amplitude at least 50% of the peak on current was expected to rise with the same time course as the measured step response of the recording system (see below). Further, recordings with very large ionic currents (> 2.5 nA) were rejected to avoid errors due to series resistance.

To allow the interpretation of the rapid gating events reflected in the recordings of ionic tail currents and reactivation time courses, the step response of the recording system, including the filter, was determined by injecting a step of current into the patch clamp head stage using the test facility of the EPC-9 and measuring the current response. At the low gains at which the macroscopic ionic and gating currents were measured (500 M Ω feedback resistor), the response time, defined as the time required for the current to reach 50% of its peak in response to a step current input, was found to be 40 and 25 μs at the 10 and 15 kHz filtering bandwidths used for most ionic current measurements, respectively. Other delays in the stimulus and recording system were expected to be negligible: the stimulus filter risetime was set at 2 μs for measurements of tail currents and reactivation time courses, while the patch membrane charging time constant was expected to be below 1 μs . To account for the total delays, the recorded current traces were offset in time by three sample intervals. In the measured time course of the step response of the recording system, it was also determined that an additional approximately three sample intervals were required for the step response to settle to near its final level. Thus, an additional three sample intervals were always ignored in the fitting of exponentials to the tail current and reactivation time courses.

The time courses of the macroscopic ionic and gating currents were fitted to the sums of exponentials by least squares within the Igor data analysis program (WaveMetrics, Lake Oswego, OR). The derived parameter estimates were consistently independent of the initial guesses supplied.

In the text, errors in all measured quantities are given as the mean \pm SEM.

Measurement of Single-Channel Ionic Currents

Single-channel recordings were made in inside-out patches in response to step depolarizations from a -93 -mV holding potential. Patch pipettes were pulled from 7052 glass (Garner Glass, Claremont, CA) with 1–2- μm tip diameters (4–10 M Ω resistance). The recording solutions were identical to those used in the measurements of macroscopic ionic currents. Filtering and sampling frequencies were variable, appropriate for the amplitude of the single-channel activity at a given voltage. Leak subtraction was performed by subtracting an average of 8–20 of the nearest null traces. To allow the measurement of a large number of single channel sweeps, the pulse frequency was set to be high (1–5 Hz); however, there was no indication of slow inactivation, which would have caused a time-dependent increase in the number of

¹Abbreviations used in this paper: CTx, charybdotoxin; NMDG, *N*-methyl-D-glucamine; WT, wild type.

null traces. The displayed single channel data are filtered at the frequencies used for the event detection, as described below.

The single-channel activity apparently arose from *Shaker* channels since (a) no such single channel activity was observed in patches in which CTx was included in the pipette, and (b) the ensemble averages of WT's single-channel current traces were kinetically identical to the macroscopic currents in patches from oocytes injected with 50–100-fold more cRNA. Infrequently, a patch would display other single-channel activity, but this activity was easily distinguishable from *Shaker*'s in its voltage-dependence, kinetics, and conductance properties.

The analysis of the equilibrium single-channel closed and open times was performed with the TAC single-channel analysis program, which is based on THAC (Sigworth, 1983). Data were filtered with a digital Gaussian filter to achieve an appropriate signal-to-noise ratio, and event detection was performed using the standard half-amplitude threshold analysis (Colquhoun and Sigworth, 1995). Complicating the analysis of the single-channel events was the presence of apparent subconductance activity (Hoshi et al., 1994). The event detection for a given trace was stopped at the time point at which the channel first exhibited such behavior. Ignoring these data was unlikely to introduce a significant error in our results since subconductance activity was relatively infrequent: in one patch recording of 613 consecutive traces of single channel activity at +27 mV, the open channel spent only 14% of the total 16.6 s of recorded open time at a subconductance level. Here a subconductance level was defined to be an amplitude level smaller than 75% of the most common amplitude level.

For the construction of closed- and open-time histograms, the deadtime (T_d) for a given analysis filtering frequency f_c was taken to be $T_d = 0.179/f_c$ and short-event durations were adjusted appropriately for Gaussian filtering as described (Colquhoun and Sigworth, 1995). Closed and open times were binned logarithmically and the square root of the number of events was plotted (Sigworth and Sine, 1987). The minimum-duration bin for each histogram was set to be the deadtime corresponding to the analysis filtering frequency used for the event detection. The event histograms were fitted to a mixture of exponential components with the amplitudes and time constants adjusted using the binned maximum likelihood method (Sigworth and Sine, 1987). The number of exponential components fitted to the histograms was determined by the likelihood ratio test for nested models (Horn and Lange, 1983), which can be applied to the problem of comparing fits with different numbers of exponentials (McManus and Magleby, 1988).

Accounting for Three Artifacts

In the following section, we describe how we accounted for three additional potential artifacts that could affect our interpretation of the data.

Effects of different recording solutions. While most of the recordings were made with the bath and pipette solutions indicated above, different solutions were sometimes used to facilitate certain types of the measurements. For these instances, it was important to show that changing the recording solution had no effect on activation gating.

First, to allow the measurement of large inward ionic tail currents at very hyperpolarized voltages (see Fig. 7 A), measurements were routinely performed while replacing 14.3 mM of the NMDG⁺ in the pipette with an equimolar amount of K⁺. High concentrations of external K⁺ have been shown to alter the ionic tail currents for *Shaker* channels (Stefani et al., 1994), and, indeed, we found that 140 mM K⁺ in the pipette slowed the decay of the ionic tail currents by a factor of two and caused a -15-mV

shift in the voltage dependence of P_o . However, tail-current recordings made at -93 mV in four patches with 14.3 mM external K⁺ had decay time constants identical to those measured in five patches with no K⁺ added to the pipette solution. In our analysis, we therefore assume that external K⁺ up to 14.3 mM has no effect on channel gating.

Secondly, some of the gating current measurements that we report were made with Cs⁺ replacing K⁺ in the bath. Cesium was originally used in many of our recordings since it is much less permeant in *Shaker* channels (Heginbotham and MacKinnon, 1993). However, Cs⁺ was observed to cause small changes in the properties of the gating currents at intermediate voltages (near -50 mV): Cs⁺ shifts, by -15 mV, the voltage range where a slow exponential component appears in the on gating current, and also shifts, by -15 mV, the prepulse voltages after which off gating currents begin to decay slowly. Since these phenomena are associated with channel opening (Bezanilla et al., 1991, 1994; Zagotta et al., 1994a), we take these changes to mean that Cs⁺ alters some of *Shaker*'s late gating transitions. Cs⁺, however, apparently does not alter the early gating transitions. Parallel measurements of gating currents made with bath K⁺ and Cs⁺ showed that gating currents induced by voltage pulses between -73 and -113 mV are unaffected by bath Cs⁺. Our analysis of gating currents at $V \leq -93$ mV thus includes data obtained in Cs⁺ as well as K⁺ (Fig. 6 A). It should be noted that the liquid junction potential in the Cs⁺/NMDG⁺ solutions (-12 mV) was essentially the same as that for K⁺/NMDG⁺ solutions.

Nonstationarities in channel behavior. Sigg et al. (1994a) have reported that the decay of *Shaker*'s ionic tail currents recorded in excised membrane patches slows by a factor of ~3 during the first several minutes after patch excision. We observed a similar time-dependent slowing in WT's tail currents. In eight patches, tail currents at -93 mV recorded at least 6 min after patch excision had decay time constants that were 2.9 ± 1.1 -fold longer than tail currents recorded less than 1 min after patch excision. Time-dependent changes were also observed in the decay of WT's off gating currents after large depolarizations, which also reflect the kinetics of channel deactivation (Bezanilla et al., 1994; Zagotta et al., 1994a). For the analysis of the macroscopic ionic tail currents and off gating currents, we therefore limited the analysis of tail currents to those measured at least 6 min after patch excision, when most of the time-dependent effects were apparently over. In seven patch recordings, in which tail currents were measured at different times up to 11 min or more after patch excision, the time-dependent slowing effect occurred with a time course that was approximated by a single exponential with $\tau = 6.2 \pm 1.5$ min.

No time-dependent effects were observed for any other macroscopic current properties. In three patches in which large changes in tail current decay rates occurred, the equilibrium voltage dependence of open probability never shifted by >3 mV and no significant changes in the measured activation time constants (at $V \geq -53$ mV) were observed. We observed no nonstationary behavior in WT's single channel activity.

Slow inactivation. A final potential problem for the interpretation of the macroscopic current time courses was slow-inactivation gating (Hoshi et al., 1991; Lopez-Barneo et al., 1993). In recordings made with 4–8-s voltage pulses to between -53 and +67 mV, macroscopic ionic currents decayed with voltage-independent kinetics that were fitted by the sum of two exponentials with time constants (at -13 mV) of 70 ± 13 and 870 ± 76 ms ($n = 7$); the 70-ms component comprised $26 \pm 19\%$ of the total amplitude. The slow inactivation time course was much slower than most, but not all, phenomena associated with activation gating. Thus, in the fits of exponentials to the channel opening time courses that are reported, an additional exponential component

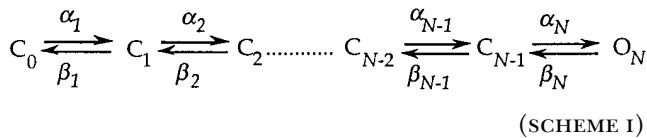
was always added that reflected the 70-ms component of the slow inactivation process.

RESULTS

The goal of this study is to identify kinetic transitions in activation gating and assign rate constants for the WT channel. Experiments were designed to isolate, as much as possible, the rates of individual steps in the activation process. In the first studies that we describe, we make use of data obtained at voltage extremes to study kinetic constants. We consider forward rates, assigning values and voltage dependences to the first forward rate α_1 , the limiting rate at large positive potentials α_p , and the final opening rate α_N . An estimate for the voltage dependence q_{ad} of intermediate steps is also obtained. Similarly, the first and the last two backward rates β_1 , β_N , and β_{N-1} are determined, along with an estimate of the "average" rate of intermediate steps β_d . In the second group of studies, we characterize the transitions to several channel-closed states that are distinct from those traversed in the depolarization-induced activation process.

General Framework

We assume a discrete, homogenous Markov model for activation gating. Thus, activation is taken to involve transitions between discrete closed and open states separated by large energy barriers. For a sequential gating scheme, this framework can be depicted as



The forward and backward rates α_i and β_i are taken to be exponential functions of the membrane potential V , scaled by the partial charges $q_{\alpha i}$ and $q_{\beta i}$,

$$\alpha_i(V) = \alpha_i(0) e^{q_{\alpha i} V / kT}$$

$$\beta_i(V) = \beta_i(0) e^{q_{\beta i} V / kT} \quad (1)$$

(Terms with higher powers of V in the exponent are not included because any charge movement with the expected properties, if present, is very small; see Sigworth, 1994.) The gating charge movement accompanying a transition from state $i - 1$ to state i is then given from the partial charges as

$$z_i = q_{\alpha i} - q_{\beta i} \quad (2)$$

Within this framework, we estimate the forward and backward rate constants α_i and β_i for various gating transitions. Many of the current measurements were made at voltages where we could presume that either

forward or backward rates predominate. Following Zagotta et al. (1994a), we define three voltage ranges. Forward rates are presumed to predominate in the depolarized voltage range, where WT's equilibrium P_o and charge movement Q saturate. In WT's $P_o - V$ and $Q - V$ relations in Fig. 1, this appears to occur above -20 mV. (Although small changes in channel P_o continue at higher voltages, this property reflects the voltage dependence of a transition to a state that is not in the activation path and which carries only $\sim 0.3 e_0$ of charge; Zagotta et al., 1994a.) Backward rates are presumed to predominate at all voltages where most channels reside amongst the earliest closed states at equilibrium. These hyperpolarized voltages were taken to be $V \leq -90$ mV because only 8% of WT's charge movement occurs negative to -90 mV. A third voltage range, activation voltages, between -90 and -20 mV, is the range in which WT's channel P_o and charge movement are undergoing most of their changes.

Given the special condition that all of the backward rates in Scheme 1 are negligible, information about the forward rate constants in any sequential scheme can be obtained from a simple analysis of the time course of the open probability. At depolarized voltages, where we

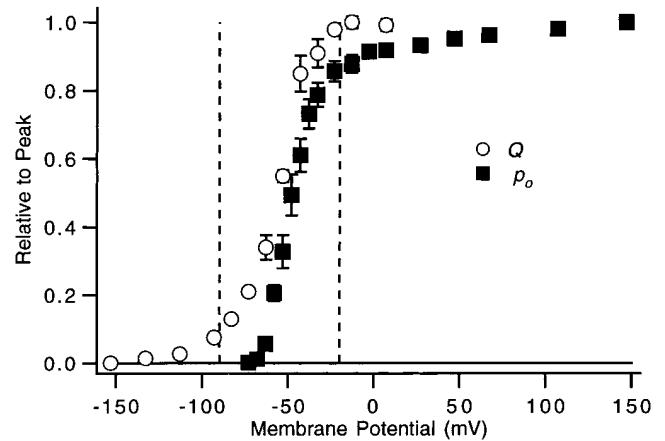


FIGURE 1. Voltage dependence of relative channel open probability P_o and charge movement Q . Relative P_o estimates (■) at $V \leq +67$ mV were derived from measurements of ionic currents made using a double pulse protocol, in which currents were measured at a fixed amplitude voltage pulse (at -13 or $+7$ mV) that followed different test pulses. The values at $+107$ and $+147$ mV were obtained by measuring the magnitude of the current relaxation elicited by voltage jumps from $+67$ mV (in experiments similar to those illustrated in Fig. 12 A). Each plotted value reflects one to eight experiments. Relative Q estimates (○) were obtained as described previously (Schoppa et al., 1992), by numerically integrating the on gating current at each voltage. Each value reflects three to five experiments. The vertical dashed lines at -20 and -90 mV mark the boundaries of the defined hyperpolarized ($V \leq -90$ mV), activation (-90 mV $< V < -20$ mV), and depolarized ($V \geq -20$ mV) voltage ranges.

assume $\beta_i \rightarrow 0$ for all i , the mean latency to arrive at the open state O_N is given by

$$t_1 = \sum_{i=1}^n \alpha_i^{-1}. \quad (3)$$

Now suppose that one of the rates, α_j , is much smaller than the others. Then the time course of channel activation can be approximated by the exponential function

$$P_o(t) \approx \begin{cases} 0, & t \leq \delta \\ 1 - e^{-(t-\delta)/\tau}, & t > \delta, \end{cases} \quad (4)$$

with time constant $\tau = \alpha_j^{-1}$ and with a time delay equal to the latency due to the other steps,

$$\delta = \sum_{i \neq j} \alpha_i^{-1}. \quad (5)$$

The approximate time course given by Eq. 4 has a mean latency that is equal to t_1 ; however, the time course is correct only as the limiting rate α_j becomes much smaller than the other rates. Useful estimates of the limiting rate and of δ can nevertheless be obtained from fits of Eq. 4 when the limiting rate differs little

from the other rates. This is illustrated in Fig. 2, where fits were made to the “upper half” of the time course, starting at the time when P_o is equal to half of the final value. In Fig. 2 A, an “ n^4 ” scheme where the next slowest rate is only twice that of the slowest one, the limiting rate is estimated with 11% error, while δ is estimated within 1%. Fig. 2 B demonstrates the worst case, in which no rate constant is smaller than the others. Here, the limiting rate is underestimated by a factor of two, while the error in δ is only 20%. Similar deviations between the measurements and theory are obtained from sequential schemes with more transitions. For an “ n^8 ” scheme, the deviations in the measured and predicted τ^{-1} and δ are only 13 and 1%, respectively; for eight equivalent rates, the deviations in τ^{-1} and δ are 61 and 13%. These results suggest that fits of Eq. 4 to activation time courses for sequential models can yield reasonable first-pass estimates of the rate-limiting rate constant, though this rate will tend to be underestimated in cases where several rates are comparable in magnitude. Information about the other transitions is also obtained with surprisingly good accuracy from the delay value.

The approximation of Eq. 4 can also be used to obtain a simple characterization of dwell times during ac-

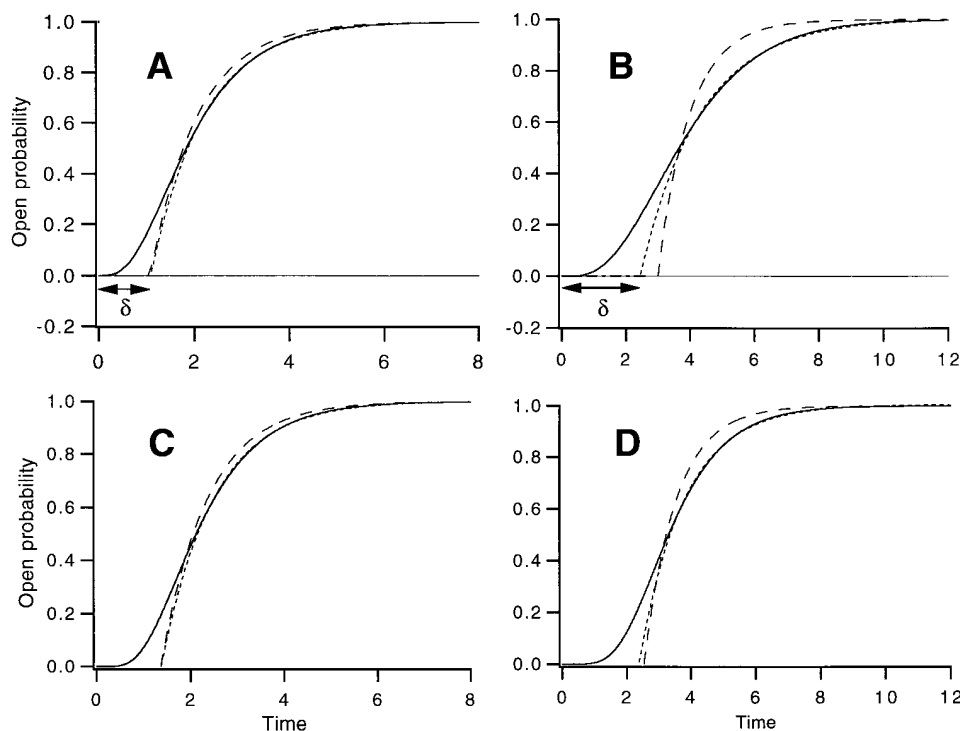
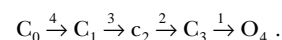


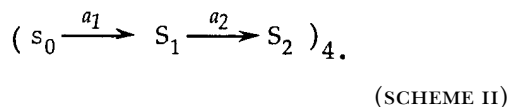
FIGURE 2. Fits of a single exponential function and delay (Eq. 4) to the time course of open probability P_o predicted by different models. (A) Fits to the time course of P_o (solid curve) from the n^4 scheme



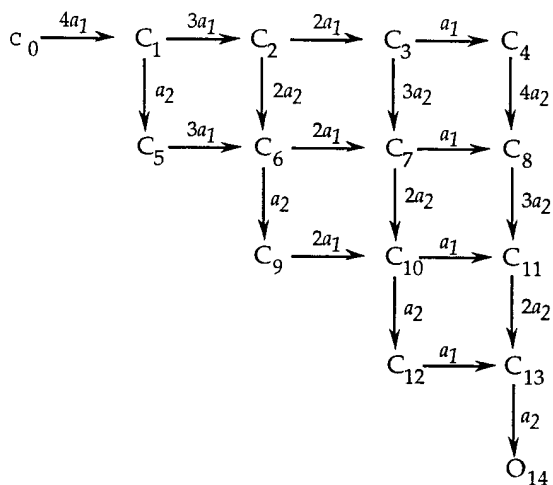
Note that the order of rate constants in this scheme does not influence the time course. A fit of Eq. 4, taking only points where $P_o \geq 0.5$, is shown as the dotted curve; it yields $\tau^{-1} = 0.89$ and $\delta = 1.09$. The values expected from the approximate theory, $\tau^{-1} = 1$ and $\delta = 1.083$, yield the dashed curve. (B) Fits to the time course from the same scheme but with all four rate constants equal to 1. The fit (dotted curve, fitted for $P_o \geq 0.5$) yielded $\tau^{-1} = 0.53$ and $\delta = 2.45$; the expected values are $\tau^{-1} = 1$ and $\delta = 3$ (dashed curve). (C) Fits to the time course of P_o from Scheme II, in which each of four independent subunits un-

dergoes two transitions, with the forward rate constants a_1 and a_2 equal to 1 and 4, respectively. The fit (dotted curve, fitted for $P_o \geq 0.5$) yielded $\tau^{-1} = 0.89$ and $\delta = 1.38$. The expected values are $\tau^{-1} = 1$ and $\delta = 1.37$ (dashed curve); these were obtained from the mean latency to opening t_1 that was computed by use of a recursive subroutine as the expectation value over all possible paths in Scheme II of the sum of dwell times in states in each path. (D) Fits to the time course from Scheme II with a_1 and a_2 both equal to 1. The fit (dotted curve) yielded $\tau^{-1} = 0.71$ and $\delta = 2.38$; the expected values are $\tau^{-1} = 1$ and $\delta = 2.55$ (dashed curve).

tivation in branched models. Consider a model like that of Zagotta et al. (1994b) in which four independent subunits each undergo two steps,



When this scheme is expanded, it is seen that there are many distinct paths (14 in all) leading from closed state C_0 to the open state O_{14} .



The mean latency t_l can be computed as a weighted average of the time spent in each path, with the weights being the probabilities of the paths. The time spent in each path is the sum of the dwell times in each state of the path.

Fig. 2 C shows an example of fits to the time course for this scheme in the case where $a_1 = 1$ and $a_2 = 4$, yielding $t_l = 2.369$ time units. The simple theory predicts τ to be equal to the reciprocal of the slowest rate, and the delay parameter to be given by $\delta = t_l - \tau$. A single-exponential fit (*dotted curve*) yields a value for τ^{-1} that differs by 11% from the slowest rate, and a value of δ that differs only 1% from the theoretical value. Fig. 2 D demonstrates the most difficult case, in which $a_1 = a_2$. As in the corresponding case of a sequential scheme (Fig. 2 B), the error in the time constant is moderate, $\sim 30\%$, but the error in δ is small, $< 1\%$. Thus, the parameters of a fitted single-exponential function give surprisingly good estimates for the aggregate dwell times in branched models as well as in linear models.

Estimates of Forward Rates

Estimates of α_1 . The forward rate constant α_1 for the first transition was evaluated from the time courses of ionic currents and gating currents at depolarizing voltages, as illustrated in Fig. 3. Fits of the single-exponential function (Eq. 4) to the ionic current from the 50% amplitude level to its final value yielded the “activation

time constant” τ_a and the activation delay δ_a (Fig. 3 A). From the exponential decay of gating currents at depolarized voltages, the time constant τ_{on} was determined (Fig. 3 B).

It has been shown previously that *Shaker*'s on gating current displays a rising phase (Bezanilla et al., 1994), which implies that the forward rate of the first transition is slower than subsequent transitions or that the first transition has less associated charge movement. The additional observation that τ_a and τ_{on} have similar values at voltages near 0 mV (Fig. 3 C) suggests that the first step is the slowest at these voltages, being rate limiting for both channel opening and the movement of the charge.

The relationship between τ_a and τ_{on} is shown for a five-state sequential gating scheme in Fig. 3 D. In these simulations, we set the rates of all but one of the transitions to be equivalent and fast, and varied the position of the slow step. Only the case in which the slow step was the first step does the gating current decay with a single exponential with a time constant τ_{on} that is nearly identical to the activation time constant τ_a . We also show the relationship between τ_a and τ_{on} for the branched model in Fig. 3 E (*bottom*). For the case in which we made the rate a_1 of the first “subunit transition” slow and rate limiting, the τ_a and τ_{on} values are nearly equivalent; however, for the case in which a_2 is slow, the τ_a and τ_{on} values differ by a factor of 2. The results of these simulations suggest that it is reasonable to take the similarity between τ_a and τ_{on} for *Shaker* to mean that the first gating step is indeed the slowest. Activation at depolarized voltages then mirrors channel deactivation at hyperpolarized voltages, where the similar off gating current and tail current decay time courses imply that the first steps in channel closing are the slowest at these voltages (Bezanilla et al., 1991; Zagotta et al., 1994a).

An estimate of the voltage dependence of the first forward rate α_1 can be obtained from the τ_a or the τ_{on} values at voltages up to +67 mV (Fig. 3 C). The reciprocal of the τ_a values derived from ionic currents measured between -13 and +67 mV in seven different patches yielded $\alpha_1(0) = 1,200 \pm 90 \text{ s}^{-1}$ and $q_{\alpha 1} = 0.36 \pm 0.02 e_0$. As derived from τ_a , the value of α_1 might be underestimated if, as in the case illustrated in Fig. 2 B, other transitions have very similar rates. However, the close correspondence of τ_a and τ_{on} argues against the presence of this error.

Estimate of α_p . If one or more transitions have forward rates with smaller voltage dependences than α_1 , one of these should be rate limiting at sufficiently high voltages, and should be reflected in the voltage dependence of τ_a at very large positive voltages. Thus, we obtained current recordings at voltages up to +147 mV (Fig. 4 A). The analysis of the channel opening time

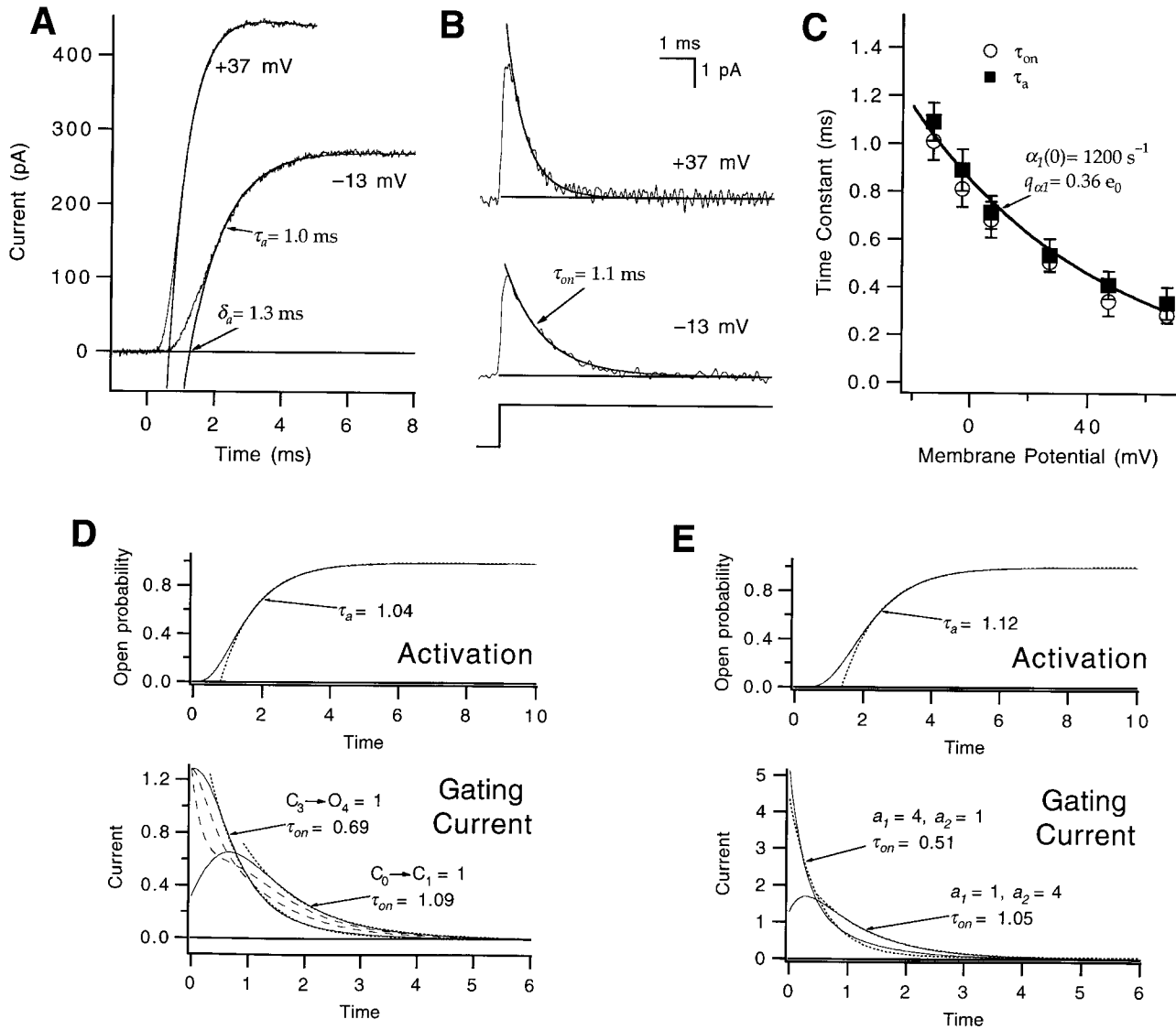


FIGURE 3. Estimate of α_1 . (A) Macroscopic ionic currents at -13 and $+37$ mV were fitted to a single exponential (smooth curves) to estimate an activation time constant τ_a . Extrapolating the fitted exponential to zero current yielded an estimate of the activation delay δ_a . Patch w312. (B) The decay of WT's on gating currents at the same voltages was fitted to a single exponential (smooth curves) to estimate the decay time constant τ_{on} . Patch w212. For the fitting, a baseline was first calculated from the mean current measured at the end of the voltage pulse (horizontal lines); the fitting began at the time point at which the current had decayed by 20% from the peak value. (C) The values of τ_a (■) and τ_{on} (○) derived from the fitting have nearly equal values at voltages between -13 and $+67$ mV. Each data point reflects the average from two to eight experiments. Superimposed curve reflects the average voltage dependence of α_1 , obtained by fitting the τ_a values between -13 and $+67$ mV in seven different patches. (D) Exponential fits of the activation time courses and on gating currents for a five-state sequential scheme, as depicted in the legend for Fig. 2 A. For these simulations, the rates for all but one of the transitions was set to be 4; the slowest transition had a rate constant equal to 1. The position of the slowest transition was varied to yield the different curves. The activation time courses (top) were identical for each of the conditions; these were fitted to an exponential (dotted curve), yielding an activation time constant $\tau_a = 1.04$. The gating current time courses for each of the conditions (bottom), however, differed. For $C_1 \rightarrow C_2, C_2 \rightarrow C_3 = 1$, the decay of the currents (dashed curves) was not well described by a single exponential. For $C_3 \rightarrow C_4 = 1$, the decay of the current (solid curve) was well described by a single exponential (dotted curve), but the fitted time constant $\tau_{on} = 0.69$ was faster than τ_a . For $C_0 \rightarrow C_1 = 1$, the decay time constant $\tau_{on} = 1.09$ was similar to τ_a . (E) Exponential fits of the activation time courses and on gating currents for Scheme II, with the forward rate constants a_1 and a_2 equal to 1 and 4, respectively, or with $a_1 = 4$ and $a_2 = 1$. The two cases yielded identical activation time courses (top), which were fitted to an exponential with $\tau_a = 1.12$ (dotted curve). The two cases, however, yielded different gating currents (bottom). The decay of the current for the case of $a_1 = 1$ and $a_2 = 4$ (solid curve) was well described by a single exponential with a time constant $\tau_{on} = 1.05$, similar to τ_a . The case of $a_1 = 4$ and $a_2 = 1$, however, yielded a more complex gating current decay time course, which, when approximated by a single exponential (dotted curve), yielded a decay time constant $\tau_{on} = 0.51$ that was much faster than τ_a . In all simulations, each transition carried an equivalent charge movement.

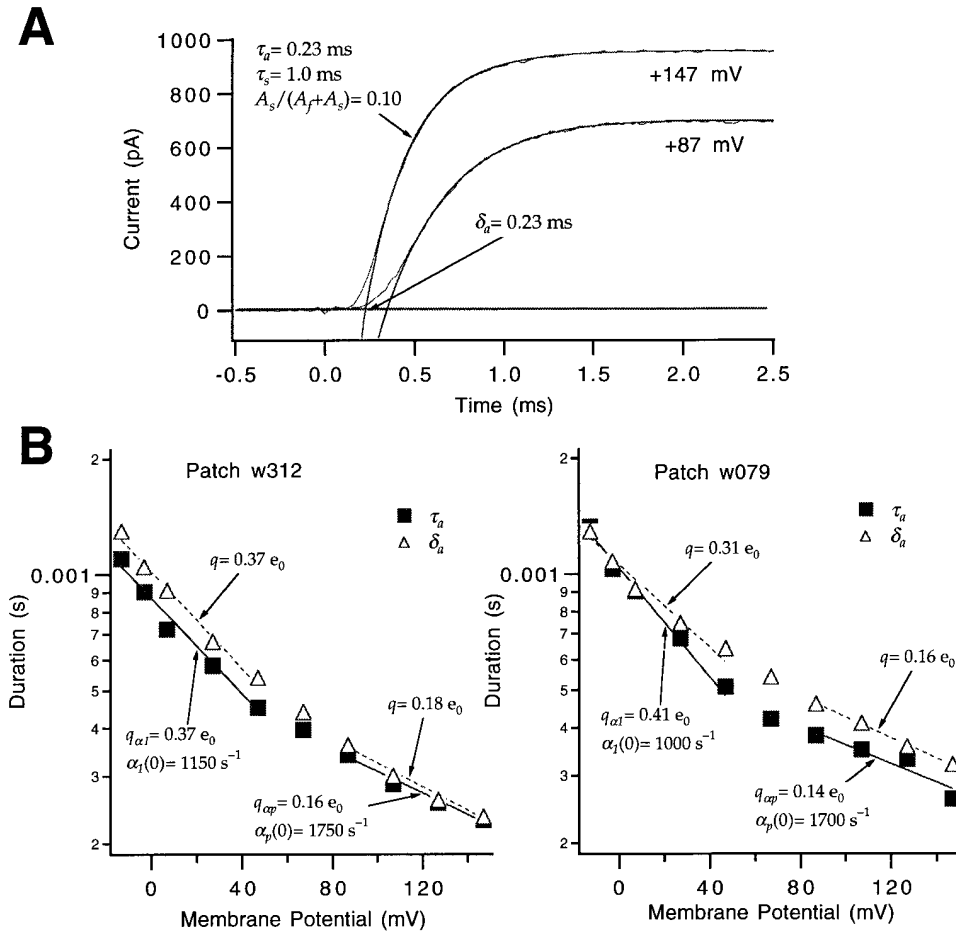


FIGURE 4. Estimate of α_p . (A) The upper half of the macroscopic ionic current time course at +87 and +147 mV was fitted to one or two exponentials (Eq. 6), respectively, to estimate τ_a and δ_a (smooth curves). Two exponentials were required at +147 mV to account for a slow relaxation that corresponds to an alternate activation path. Patch w312. (B) Voltage dependence of τ_a and δ_a taken from current measurements in two different patches (left and right). The τ_a values display shallower voltage sensitivities at high voltages. The voltage dependence of the rate α_p was estimated from the τ_a values at $V \geq +87$ mV (solid lines at $V \geq +87$ mV). The δ_a values between -13 and +147 mV also become less voltage sensitive at high voltages. Estimates of the charge q that determines the voltage sensitivity of the delay at low and high depolarized voltages, respectively, were obtained by fitting an exponential to the δ_a values at $V \leq +67$ and $\geq +87$ mV (dashed lines). These charge values will be used in a following paper (Schoppa and Sigworth, 1998b).

course at high depolarized voltages is complicated by the fact that the rising phase of the current is usually not well fitted by a single exponential. After a rapid rise, a slow “creep” up to the final value is observed at these voltages. In a more complete discussion of this phenomenon below, we will show that this slow component reflects an alternate activation path that a small fraction of the channels enter before opening. Here, to estimate the kinetics of the main activation path, the currents were fitted to the sum of two exponentials,

$$I(t) = A_f + A_s - (A_f e^{-(t-\delta_a)/\tau_a} + A_s e^{-(t-\delta_a)/\tau_s}), t > \delta_a. \quad (6)$$

τ_a was taken to be the time constant of the faster decay, whose amplitude A_f accounted for $\sim 90\%$ of the total. The log-transformed values of τ_a up to +147 mV from two patches are plotted in Fig. 4 B. These plots do not show the linear dependence on voltage expected if a single transition is rate limiting at all of the voltages; instead, the dependence of τ_a on voltage becomes increasingly shallow at high voltages. Zagotta et al. (1994a) made recordings of activation time courses only at voltages up to +50 mV, so these authors did not observe this deviation from simple behavior.

Estimates of the forward rate α_p of the rate-limiting step at high depolarized voltages were obtained as the reciprocals of τ_a values derived from the ionic current time courses measured between +87 and +147 mV, yielding $\alpha_p(0) = 2,100 \pm 100$ s⁻¹ ($n = 6$) and $q_{app} = 0.17 \pm 0.02 e_0$. It is not clear where in the sequence of gating steps this rate-limiting step occurs. The time course of gating currents at these high voltages could provide some information about this, but we did not record gating currents in this voltage range.

Estimate of α_N . Macroscopic ionic currents were measured with one additional voltage protocol to attempt to estimate the forward rate α_N of the very last step in the activation path (Fig. 5). A sequence of three voltage pulses was applied (Fig. 5 A): an initial depolarization to +47 mV to open most of the channels, a second pulse to a hyperpolarized voltage V_h (-153 mV in this case) of duration t_h to close a fraction of the channels, and a third pulse to +47 mV to reopen the channels that closed during the second pulse. In principle, for small enough t_h , channels should not have time to close to states beyond the first closed state, and the kinetics of channel reactivation should reflect the forward rate of the last transition in the activation path. This time course will be distinctly faster if the forward rate of the

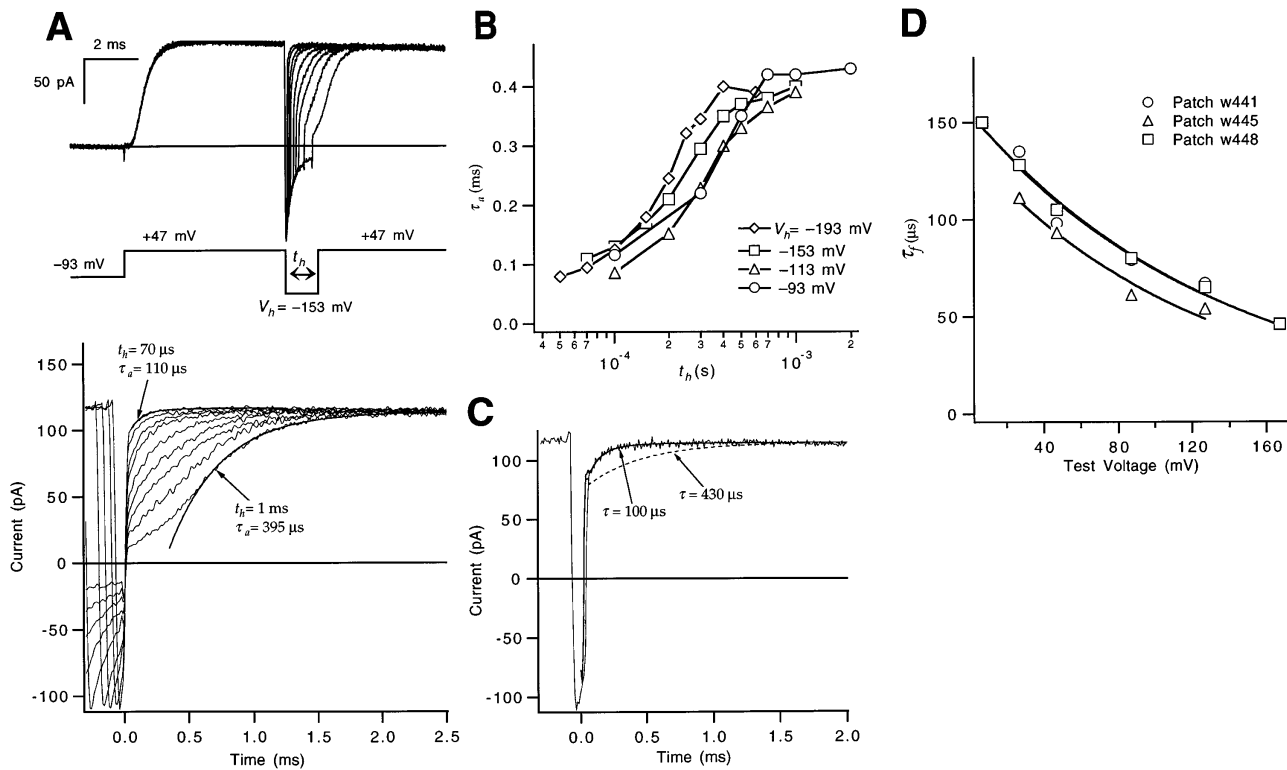


FIGURE 5. Estimate of α_N from a fast reactivation component. (A, top) WT's macroscopic ionic currents elicited by a triple-pulse stimulus, using a pair of depolarizations to +47 mV separated by a voltage step to a hyperpolarized voltage $V_h = -153$ mV. The displayed currents correspond to different hyperpolarization durations t_h between 70 and 1,000 μ s. Tail currents during the second pulse were inward since the pipette solution contained 14 mM K^+ . Data were filtered at 15 kHz. Patch w448. (bottom) The same traces are shown, but expanded and time shifted to align the start of the test pulses. The "upper half" of the reactivating current relaxations for $t_h = 70$ μ s and 1 ms have been fitted to a single exponential to estimate τ_a (smooth curves). (B) The dependence of the derived values for τ_a on the hyperpolarization duration t_h , shown for different hyperpolarization amplitudes V_h . Note that for each V_h , the fastest τ_a values appear to approach 100 μ s. All data reflect the patch in A. (C) To demonstrate that the fast reactivating component is not a recording artifact, we compare the apparent fast reactivating current in A for $t_h = 100$ μ s with two different simulated current traces reflecting Eq. 7. The solid and dashed smooth curves, respectively, correspond to $x(t)$ being a single exponential with a fast time constant $\tau = 100$ μ s (the good fit) or a slower $\tau = 430$ μ s (the poor fit). The total amplitude (-39 pA) associated with $x(t)$ was constrained by fitting the tail current at -153 mV in the same patch to the sum of two exponentials and determining the amount of decrease in current by 100 μ s after the beginning of the pulse. The impulse response $h(i)$ was determined by differentiating the step response measured at the 15-kHz bandwidth (see METHODS). (D) The fast reactivation time constant (τ_f) values at different voltages were fitted to an exponential (solid curves) to estimate the voltage dependence of α_N , yielding estimates for $\alpha_N(0)$ and q_{α_N} for each of three patches ($\alpha_N(0) = 7,600, 6,800,$ and $6,500$ s^{-1} and $q_{\alpha_N} = 0.19, 0.16,$ and 0.18 e_0). For each patch, τ_f was obtained from currents measured after a 150- μ s hyperpolarization to -153 mV. The reactivation time course for $t_h = 150$ μ s includes a small slow component (accounting for, on average, 14% of the time course) as well as the dominant fast component; the τ_f values reflect the fast time constant in fits of the reactivation time course to the sum of two exponentials:

$$I(t) = A_f + A_s - (A_f e^{-t/\tau_f} + A_s e^{-t/\tau_s}).$$

last transition is faster than that of the earlier gating steps. Zagotta et al. (1994a) measured currents using a similar voltage protocol with t_h as small as 1 ms, but we employed second-pulse hyperpolarizations that were much shorter, as short as 70 μ s. In our experiments, briefer hyperpolarizing pulses make the reactivating currents much faster (Fig. 5, A and B). Compared with the 400- μ s activation time constant τ_a taken from the reactivation time course after a relatively long $t_h = 1$ ms hyperpolarization, single exponential fits of the reactivation time courses for shorter t_h yielded τ_a values of

300, 170, and 110 μ s for $t_h = 300, 150,$ and 70 μ s, respectively.

Several lines of evidence suggest that these fast relaxations reflect genuine current changes due to gating and are not artifacts of the recording system. First, the single-exponential fits just described were performed while ignoring the first 60 μ s of the pulse, which at the 15-kHz bandwidth is longer than the settling time of the recording system (see METHODS). Second, the hyperpolarization to -153 mV produces a fast "instantaneous" current change reflecting the large change in

the driving force between -153 and $+47$ mV. In the reactivation time course after a 1-ms hyperpolarization in Fig. 5 A, this current change is clearly complete within $40 \mu\text{s}$ and distinguishable from the slower kinetics of the current changes during the reactivating pulse. As a final check, we simulated reactivating current time courses $I(t)$ by convolving theoretical functions $x(t)$ reflecting current changes due to gating, with the impulse response of the recording system $h(i)$:

$$I(t) = \sum_{i=0}^n h(i) x(t-i). \quad (7)$$

The impulse response $h(i)$ was obtained by differentiating the step response at the 15-kHz bandwidth at which these currents were measured (see METHODS) and was evaluated for $n = 15$ sample intervals. An additional constraint in this analysis was provided by the fact that an amplitude for $x(t)$ can be predicted given the measured tail current time course during the preceding hyperpolarization. When it is assumed that $x(t)$ is a single exponential with a time constant of $430 \mu\text{s}$, which is the τ_a value taken from the activation time course during the first voltage pulse, $I(t)$ poorly reproduces the data; but an exponential $x(t)$ with a time constant of $100 \mu\text{s}$ accounts for the current time course very well (Fig. 5 C).

The $100\text{-}\mu\text{s}$ time constant at $+47$ mV is much faster than the reciprocal of the values that we calculate for both α_1 and α_p at $+47$ mV (430 and $400 \mu\text{s}$, respectively) and thus reflects a distinct forward rate. It is difficult to prove that it is the very final step that is reflected by this time constant. More careful measurements using shorter hyperpolarizations might have revealed an even faster reactivation component associated with a later step. Nevertheless, consistent with the fast component reflecting the final step is that the effect of shortening t_h on the measured reactivation time constant appears to saturate at a value near $100 \mu\text{s}$ by the shortest -153-mV hyperpolarizations used (Fig. 5 B). The same saturating relationship between t_h and τ_a is observed when V_h is varied between -93 and -193 mV, which may be expected to produce varying occupancies in the closed states near the open state.

We define the activation time constant τ_a observed for the shortest hyperpolarization ($t_h = 70 \mu\text{s}$) to be the fast reactivation time constant τ_f reflecting the final forward rate α_N . The reciprocal of τ_f at $+47$ mV gives $\alpha_N(+47) = 9,100 \text{ s}^{-1}$. The voltage dependence of α_N was evaluated by varying the voltage of the test depolarization after a short duration hyperpolarization. From the voltage dependence of τ_f in this and two other patches (Fig. 5 D), we estimate $\alpha_N(0) = 7,000 \pm 300 \text{ s}^{-1}$ and $q_{\alpha N} = 0.18 \pm 0.01 e_0$.

Estimate of q_{ad} . The long delay in *Shaker's* channel opening time course (Zagotta et al., 1994a) is expected

to reflect the forward rates of a large number of transitions. While we were unable to determine directly the forward rates of most of the transitions that come between the very first and last transitions, information about the partial charges q_{ad} associated with the forward rates of these intermediate transitions is available from the voltage dependence of the delay δ_a in the channel opening time course (Fig. 4 B). The δ_a value represents the sum of contributions from multiple steps; its voltage dependence is not well fitted by a single exponential across the wide voltage range, which is consistent with transitions with forward rates with different voltage dependences predominating at different voltages. Nevertheless, to approximate the partial charges of a large number of these transitions here, the δ_a values between -13 and $+147$ mV were fitted to a single exponential (not shown), which yielded a charge estimate of $0.25 e_0$ for q_{ad} .

Estimates of Backward Rates

Estimates of the voltage dependences of the backward rates of three transitions were obtained from the kinetics of macroscopic ionic and gating currents at hyperpolarized voltages.

Estimate of β_1 . The small fraction ($<8\%$) of the total charge movement that occurs at voltages negative to -90 mV (Fig. 1) is consistent with the idea that at these voltages channels reside among the earliest closed states at equilibrium. If it is assumed that at -93 mV, most channels reside in either the first or second closed states, the off gating currents measured with voltage pulses from -93 mV to more hyperpolarized voltages will decay with a time course given by the backward rate β_1 of the first transition. Consistent with the expected two-state behavior, the measured currents (Fig. 6 A) rise instantaneously and have a single exponential decay that becomes faster at more hyperpolarized voltages. The time constants of the single exponentials fitted to these gating currents (Fig. 6 B) in three patches yielded an estimate for a backward rate of the earliest gating step $\beta_1(0) = 190 \pm 60 \text{ s}^{-1}$ and $q_{\beta 1} = -0.53 \pm 0.03 e_0$. Numerous reports of *Shaker's* gating currents exist in the literature (Bezanilla et al., 1991, 1994; McCormack et al., 1994; Zagotta et al., 1994a), but none of these include gating currents measured with voltage steps between different hyperpolarized voltages, which are required to estimate β_1 .

The estimates of the backward rate β_1 obtained here and the forward rate α_1 obtained earlier can be compared with the Q - V relation. The charge of the first step $z_1 = q_{\alpha 1} - q_{\beta 1}$ should match the steepness of the exponential Q - V relation at extreme negative voltages. Measurements of Q obtained between -133 and -83 mV were used, where $Q/Q_{\text{max}} \leq 0.13$. Fitting the average data to an exponential function of voltage yielded an

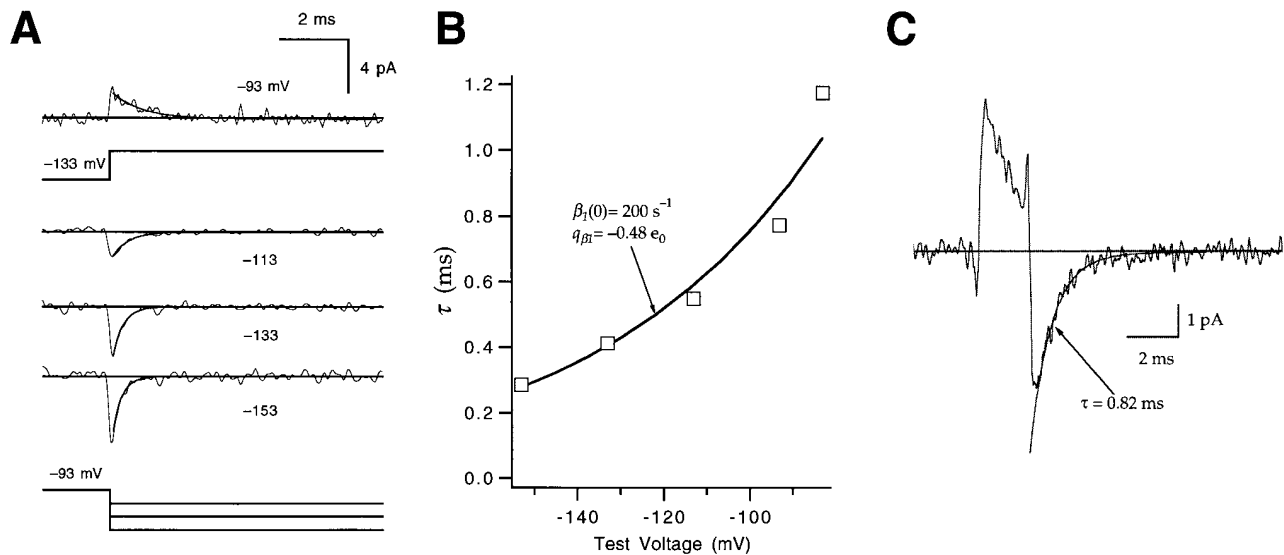


FIGURE 6. Estimates of β_1 and β_d . (A) Gating currents elicited by voltage steps between -93 and -153 mV. The current recorded at -93 mV (*top*) reflects the on current measured after a voltage step from -133 mV; the currents recorded at the -153 , -133 , and -113 -mV test voltages reflect the off current measured after voltage steps from -93 mV. Currents were fitted to a single exponential (*smooth curves*) to estimate a decay time constant τ . Patch w249. (B) To estimate β_1 , the τ values derived from the currents in A were fitted to an exponential (*solid curve*), yielding $\beta_1(0) = 200 \text{ s}^{-1}$ and $q_{\beta_1} = -0.48 e_0$. (C) The off gating current measured at -93 mV after a 2-ms depolarization to -33 mV was fitted to a single exponential with $\tau = 0.82$ ms. This time constant is similar to the reciprocal of the value of β_1 at -93 mV (0.77 ms) estimated in B, consistent with β_d being similar to β_1 at -93 mV.

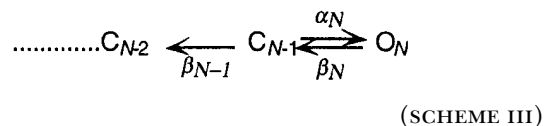
estimate of the first transition valence of $z_Q = 1.1 e_0$ (not shown). This z_Q estimate is similar to the estimate $z_1 = 0.9 e_0$ obtained from the voltage dependences of the forward and backward rates.

Estimate of $\beta_d(-93)$. It has been previously shown that Shaker's off gating currents after large depolarizations have a rising phase and decay kinetics dominated by the slow kinetics of channel closing from the open state (Bezanilla et al., 1991; Zagotta et al., 1994a). However, the off current kinetics after short depolarizations that fail to open channels are much more rapid, presumably reflecting the relatively rapid backward kinetics of the transitions that come before the last transition (Zagotta et al., 1994a). We use this rapid off current time course here to obtain an approximate estimate β_d for the backward rate of intermediate transitions. Fig. 6 C illustrates the off current measured after a short 2-ms depolarization to -33 mV. From the time integral of the gating current at this voltage, we estimate that 80% of the total gating charge movement occurs by the end of the 2-ms depolarization, indicating that most channels reside in relatively late activation states; however, from the channel opening time course, we estimate that only 15% of the channels are open. Exponential fits of the off currents after the 2-ms depolarization to -33 mV in two patches yielded time constants of 0.82 and 0.62 ms.

The decay of this off current reflects the contribution of the backward rates of many transitions, including the transitions between intermediate states that are

preferentially occupied at the end of the prepulse depolarization, and also β_1 of the first transition. The decay time constant of the current is in fact indistinguishable from the reciprocal of β_1 at -93 mV (0.77 ms), suggesting that the rate of the intermediate steps β_d is similar to β_1 at -93 mV. This analysis gives a rough estimate of $\beta_d(-93 \text{ mV}) = 1,300 \text{ s}^{-1}$.

Estimate of β_N . Zagotta et al. (1994a) made estimates of the channel closing rate β_N from macroscopic ionic tail currents measured between -60 and -140 mV. For our estimates of β_N , we chose to use tail currents measured at even more negative voltages. While the position of the Q-V relation on the voltage axis would suggest that most of the forward rates are negligible in the hyperpolarizing voltage range (≤ -93 mV), it has been shown above that the forward rate of the last transition α_N is considerably faster than the forward rates of the preceding transitions, and could have values at voltages near -93 mV that are comparable to backward rates. Indeed, according to our fits, $\alpha_N(-93) = 3,600 \text{ s}^{-1}$ is greater than $\beta_1(-93) = 1,300 \text{ s}^{-1}$. Considering a partial scheme consisting of the last three states of Scheme I,



the channel deactivation time course at these voltages might involve many reopenings from state C_{N-1} before closing further to state C_{N-2} . The large forward rate of

the last transition implies that estimates of β_N must be obtained from currents measured at voltages more negative than -93 mV.

Inward tail currents were measured between -153 and -203 mV using 14.3 mM external K^+ (Fig. 7 *A*). One criterion to determine that the tail current time course entirely reflects the channel closing rate β_N is that it should be well fitted by a single exponential, but even at the most negative voltages, the tail currents were poorly fitted by a single exponential. Assuming that the complicated channel deactivation time course reflects channel reopenings from the last closed state in the activation path, as reflected in Scheme III, esti-

mates of β_N could nevertheless be obtained by fitting the tail currents to the sum of two exponentials:

$$I(t) = A_f e^{-t/\tau_f} + A_s e^{-t/\tau_s}, \quad (8)$$

with the faster time constant τ_f reflecting β_N at sufficiently negative voltages.

In practice, only tail currents at $V \leq -153$ mV were considered in this analysis. At these voltages, τ_f displays the single-exponential dependence on voltage expected for β_N (Fig. 7 *B*). Additionally, the amplitude A_f (Fig. 7 *C*) of the fitted fast exponential increases monotonically below -153 mV, expected for a tail current time

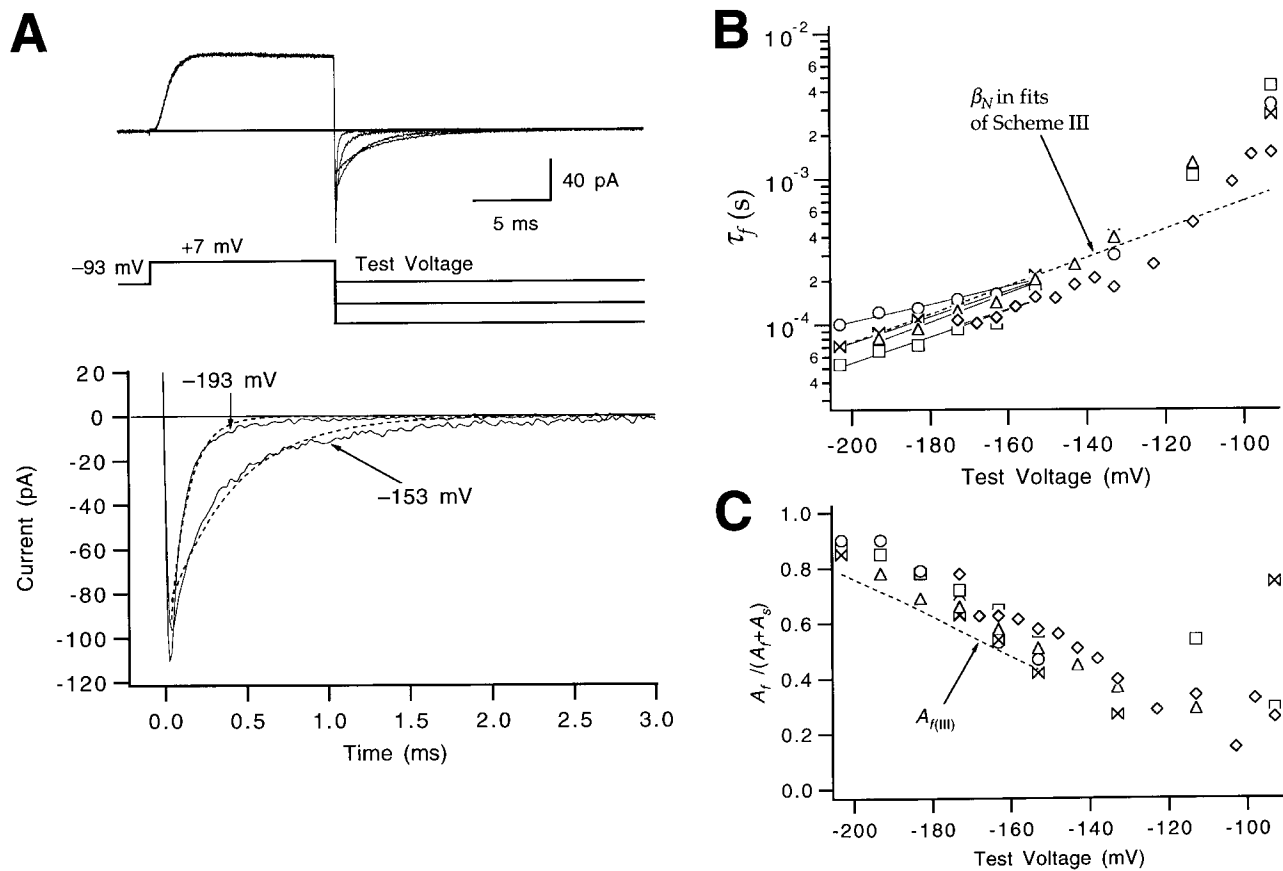


FIGURE 7. Estimate of β_N . (*A, top*) Inward macroscopic ionic currents elicited by a fixed prepulse to $+7$ mV followed by test pulses to various hyperpolarizations between -93 and -193 mV. Filtering at 15 kHz. Patch w448. (*bottom*) A single exponential (*dashed curves*) poorly accounts for the decay of the tail currents at -153 and -193 mV. (*B*) An estimate of β_N was obtained from the faster time constant τ_f in fits of the tail currents at $V \leq -153$ mV to the sum of two exponentials (Eq. 8). Values reflect five different experiments, and estimates for $\beta_N(0)$ and q_{β_N} were derived from each of the patches (*solid lines*). These estimates are similar to β_N (*dashed line*) derived from fits of Scheme III to the tail current and C_{N-1} occupancies in Fig. 8. (*C*) Voltage dependence of the relative amplitude of the τ_f component in fits of the tail currents in the same five patches to Eq. 8. The superimposed dashed curve reflects the amplitude $A_{f(III)}$ of the faster of two tail current relaxation components predicted by Scheme III, assuming values for β_N and β_{N-1} derived from the fits in Fig. 8. For $\alpha_{N-1} = 0$, the amplitude is given by

$$A_{f(III)} = \frac{\beta_N}{(\lambda_s - \lambda_f)} \left(1 + \frac{\lambda_s}{\beta_N} \right).$$

Here, λ_f is the faster relaxation eigenvalue that approaches $-\beta_N$ at very negative voltages.

course that reflects channel reopenings from the last closed state in the activation path but reflecting increasingly fewer reopenings at more negative voltages. The reciprocal of the τ_f values at different voltages below -153 mV from five separate patches yielded estimates of $\beta_{N-1}(0) = 290 \pm 90 \text{ s}^{-1}$ and $q_{\beta N} = -0.50 \pm 0.04 e_0$.

Estimate of β_{N-1} . If WT's channel deactivation time course is determined at most voltages by the channel closing rate and by reopenings from the last closed state C_{N-1} , this time course provides one way to estimate the backward rate β_{N-1} from the penultimate state. A second measure of β_{N-1} is provided by the reactivation time courses (Fig. 5 A). The amplitude of the fast reac-

tivation component should reflect the occupancy in C_{N-1} during the preceding hyperpolarization. The voltage dependences of the rates of the transitions out of C_{N-1} , including β_{N-1} , will determine the way in which this amplitude varies with the duration t_h and amplitude V_h of the preceding hyperpolarization.

Fig. 8 A illustrates the strategy we used to estimate the size of the fast component in the reactivation time course. In this analysis, we used an observation made in a different experiment, that changing the amplitude of a prepulse has a negligible effect on the kinetics of the final approach of the measured ionic current, estimated by τ_a . (These data are not shown here, but see Fig. 18 B in

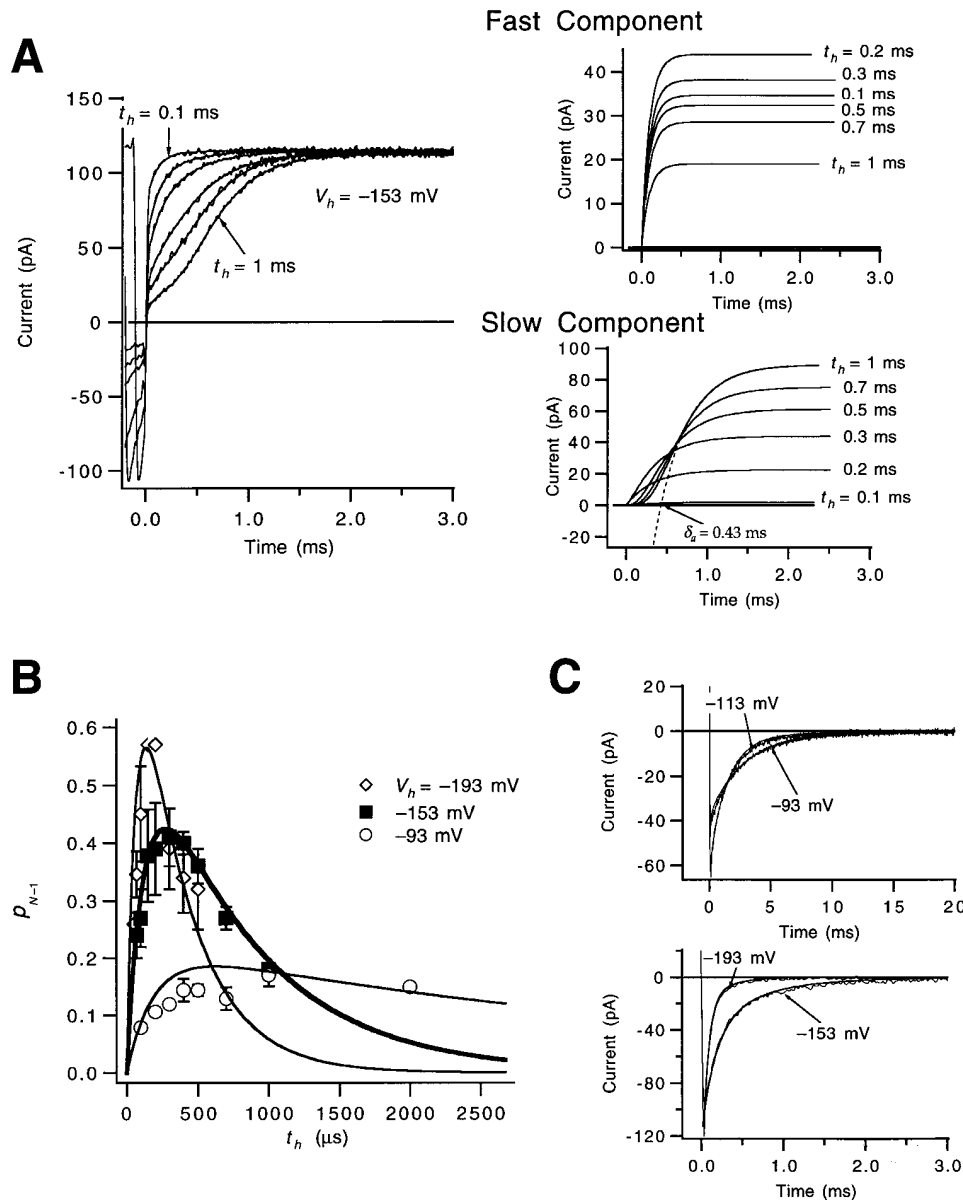


FIGURE 8. Estimate of β_{N-1} . (A) Separation of the reactivation time course into fast and slow components. Selected current traces in Fig. 5 A are shown for t_h between $100 \mu\text{s}$ and 1 ms. The time course of the fast component, reflecting channels reopening from C_{N-1} , and the slow component, reflecting channels reopening from all closed states that precede C_{N-1} , were approximated by fits of Eq. 9 (smooth curves). In the fitting, the value for α_N was fixed to the mean value derived from the reactivation time courses in Fig. 5 D. From the slow component, we derived an estimate of the delay δ_a (shown for $t_h = 1$ ms; dashed curve). (B) The occupancies in C_{N-1} derived from the reactivation time courses, as well as tail currents (C), were fitted to Scheme III (superimposed smooth curves) to obtain estimates of β_{N-1} and β_N . The occupancy p_{N-1} in C_{N-1} for different amplitude V_h and duration t_h was obtained from fits of Eq. 9 to the reactivation time course as $p_{N-1} = A_f / (I_{\text{inst}} + A_f + A_s)$; that is, taking A_f to reflect the amplitude of current due to the return of channels from C_{N-1} to the open state. This expression for p_{N-1} is approximate, but is expected to hold in this case. Each of the data points reflects one to four experiments. The parameter estimates obtained were: $\beta_N(0) = 150 \text{ s}^{-1}$, $q_{\beta N} = -0.57 e_0$, and $\beta_{N-1}(0) = 320 \text{ s}^{-1}$, $q_{\beta_{N-1}} = -0.30 e_0$. In the fitting, α_N was fixed to mean estimate value for α_N (Fig. 5 D); all channels were assumed to reside in the open state at the beginning of the test pulse.

Schoppa and Sigworth, 1998*b*). This result suggests that a reasonable approximation to the fast and slow components in the reactivation time course is the function

$$I(t) = I_{\text{inst}} + A_f(1 - e^{-\alpha_N t}) + A_s(1 - e^{-\alpha_s t})^r. \quad (9)$$

Varying the exponent r in the third term (while allowing it to take fractional values) yields an opening time course with varying amounts of delay, but with a nearly invariant final approach. The fits of Eq. 9 to the reactivation time courses in Fig. 8*A* have been separated into the respective fast and slow components. Increasing t_h from 100 to 200 μs yields a larger fast current, but the magnitude of this current decreases with even longer t_h , reflecting channels entering closed states that precede C_{N-1} during the hyperpolarization. For the slow component, increasing t_h produces a monotonic increase in amplitude, and also a longer delay, reflecting channels entering into relatively early closed states.

Estimates of β_{N-1} were then obtained by simultaneously fitting the three-state Scheme III to the time course of occupancy in C_{N-1} (Fig. 8*B*), estimates of which were derived from the amplitude of the fast reactivation component, as well as to tail currents (Fig. 8*C*). We restricted our analysis to voltages lower than -90 mV, where we assume that the tail current and occupancy time courses are functions of just α_N , β_N , and β_{N-1} ; that is, we take the reverse rate β_{N-2} to be much greater than the forward rate α_{N-1} , so that only reverse transitions occur out of C_{N-2} . In the fitting, α_N was fixed to the estimate obtained in Fig. 6, but β_N was allowed to vary along with β_{N-1} . Good fits of the tail current time courses and the derived occupancy estimates are obtained with the parameter estimates for β_N and β_{N-1} indicated in the legend. The smaller estimate for the charge $q_{\beta_{N-1}}$ compared with q_{β_N} accounts for the relatively higher occupancies in C_{N-1} at the most hyperpolarized voltages (Fig. 8*B*). We note that the derived estimates for $\beta_{N-1}(0)$ and $q_{\beta_{N-1}}$ may be too large if the assumption that β_{N-2} is much greater than α_{N-1} at $V \leq -93$ mV is not valid.

The fits of the data in Fig. 8 to Scheme III are expected to provide a more reliable estimate of β_N than that derived from fitting the tail currents to the sum of two exponentials in Fig. 7. However, the estimate for β_N derived from the fits of Scheme III is nearly identical to that derived directly from the tail currents (Fig. 7*B*). Additionally, the fast tail current component predicted by Scheme III has approximately the same amplitude as the faster component in the two-exponential fits of the tail currents (Fig. 7*C*). These observations confirm our direct estimates of β_N .

Estimate of q_{β_d} . A measure of the partial charge q_{β_d} associated with the backward rates of intermediate transitions was obtained from measurements of macroscopic ionic currents, using a strategy that is analogous to that used above to estimate q_{ad} . In that case, the voltage de-

pendence of the delay in channel activation gave a rough estimate of the voltage dependence of the underlying rate constants of intermediate transitions. Here we measure the activation delay as initial state occupancies are varied using repolarizing pulses of duration t_h and amplitude V_h that follow an initial depolarization that loads the channels into the open state. Let the initial occupancy of state i be p_i and let α_i be the forward rate from state i to state $i + 1$. Then Eq. 5 can be generalized to give the delay with arbitrary occupancies,

$$\delta_a = \sum_{i=0}^{N-1} p_i \left(\sum_{\substack{k=i+1 \\ k \neq j}}^N \alpha_k^{-1} \right) \quad (10)$$

where again we assume the unidirectional sequential Scheme I and that rate α_j is rate limiting. The dependence of δ_a on t_h will reflect the time dependence of the occupancies during the hyperpolarizing pulse and therefore depend on the backward rates of the transitions that contribute to the delay. The dependence on V_h of this accumulation will be a function of the partial charges that determine these backward rates.

The analysis of the accumulation of the delay requires defining three parameters. The first is the delay δ_a derived by fitting a single exponential to the slow component in the reactivation time course (Fig. 8*A*), which has been approximated by the second term in Eq. 9. The second parameter is $\tau_{\text{acc}}(V_h)$, which is the time constant of a single exponential fit to the dependence of δ_a on t_h at a given V_h (Fig. 9). The third parameter is the estimate of the charge q_{acc} that reflects the voltage dependence of the accumulation of the delay, obtained by fitting the τ_{acc} values to an exponential function of V_h (Fig. 9*B*).

Changing the hyperpolarization voltage V_h from -93 to -193 mV (Fig. 9*A*) causes the delay to accumulate more quickly, which is expected for backward rates with associated negative partial charges. Notably, however, the time course of the accumulation of the delay is only about twice as fast at -193 as at -93 mV, consistent with backward rates having only small partial charges. Evaluating reactivation time courses for various V_h and t_h in four patches, the $\tau_{\text{acc}}(V_h)$ values across the voltage range showed a voltage dependence corresponding to a charge of $-0.24 e_0$ (Fig. 9*B*), which we take as an estimate of q_{β_d} . Additionally, we can use this estimate of q_{β_d} to derive an estimate of the rate $\beta_d(0)$ at 0 mV, given the estimate of $\beta_d(-93) = 1,300 \text{ s}^{-1}$ obtained above from gating currents. This gives $\beta_d(0) = 540 \text{ s}^{-1}$.

Transitions to States that Are Not in the Activation Path

Up to this point, we have characterized the transitions that the *Shaker* channel undergoes in the depolarization-induced activation process. However, Hoshi et al.

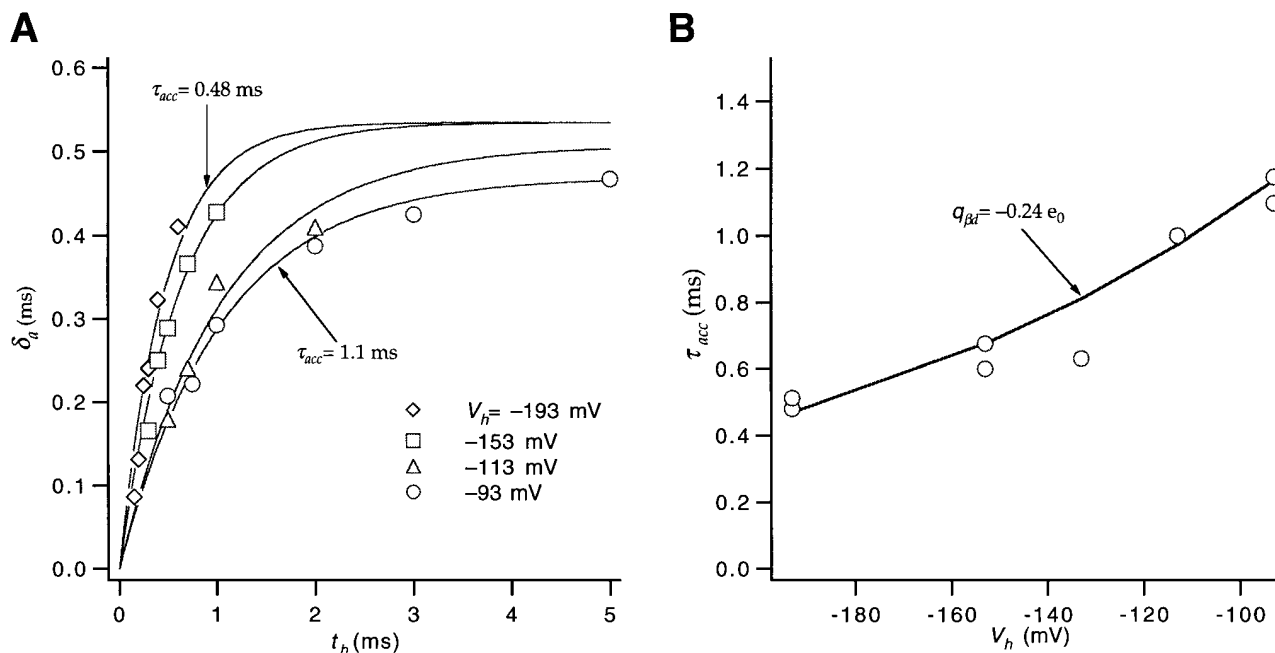


FIGURE 9. Estimate of q_{Bd} . (A) Values of δ_a taken from the slow component in the reactivation time courses (shown in Fig. 8 A), for hyperpolarizations of different amplitude V_h and duration t_h . For each V_h , the time course of the accumulation of the delay for increasing t_h was approximated by a fit of the δ_a values to a single exponential (solid curves), yielding τ_{acc} . The fitted exponential was constrained to begin at zero. The amplitude was fixed to have the value of δ_a measured from the current elicited by the first of the three voltage pulses in the triple pulse protocol (starting from a -93 -mV holding potential). For $V_h = -113$, -153 , and -193 mV, the amplitude was multiplied by a scaling factor to account for the fact that prepulses to voltages more negative than -93 mV yield a slightly longer delay in the channel opening time course. All data except for $V_h = -93$ mV come from the same patch (w448). (B) Values of τ_{acc} for different V_h were fitted to an exponential (solid curve) to estimate a charge $q_{Bd} = -0.24 e_0$. Values reflect pooled measurements made in four different patches.

(1994) have shown from Shaker's single channel data that there are at least two additional closed states, called C_f and C_i , into which the channel enters only after it has opened. The state C_f corresponds to a predominant, fast 200–300- μ s component in their single channel closed dwell-time histograms at depolarized voltages, and the other closed state C_i accounts for a voltage-independent, 1–2-ms component in the closed time histograms at depolarized voltages. In the following, we use a combination of single channel and macroscopic current measurements to further characterize the transitions to these additional states.

We begin by outlining the general properties observed in our single channel measurements at depolarized voltages. As was observed by Hoshi et al. (1994), we find that the channel opens quickly after the beginning of a voltage pulse (Fig. 10 A) and remains open for most of the trace, occasionally closing briefly into short-lived closed states. Infrequently, the channel displays longer closures (see the third trace at $+67$ mV). The closed time histograms constructed from our single channel activity are always fitted by a mixture of three exponentials (Fig. 10 B), including one large-amplitude component with a very fast ($\tau_1 = 40$ – 100 μ s) time constant, a second component with an intermediate amplitude and duration ($\tau_2 = 200$ – 500 μ s), and a third component

with a 1–3-ms time constant (τ_3) and a very small amplitude (comprising $\sim 1\%$ of the closures). Our fit of two exponentials to closures with durations of < 500 μ s differs from the single exponential fitted to these closures by Hoshi et al. (1994). It is difficult to interpret the voltage dependences of the two faster closed time components (Fig. 10 D), since the rapid closures are near the limit of time resolution and, additionally, the two rapid closed-time components are not well resolved from each other. The third, slowest component has a voltage-independent duration and corresponds to the C_i closures observed by Hoshi et al. (1994).

As shown previously (Hoshi et al., 1994), the open times (Fig. 10 C) are well fitted by a single exponential with time constants near 3 ms, consistent with the presence of a single open state. The measured open times display little voltage dependence (Fig. 10 E). No effort was made to correct the open times for missed fast closures because the missed event correction would rely on the amplitude and time constant estimates for the fastest closures, which are quite unreliable.

Characterization of the Transitions to C_i

The first new property that we assign to C_i is that it is a state that can be entered from not only the open state

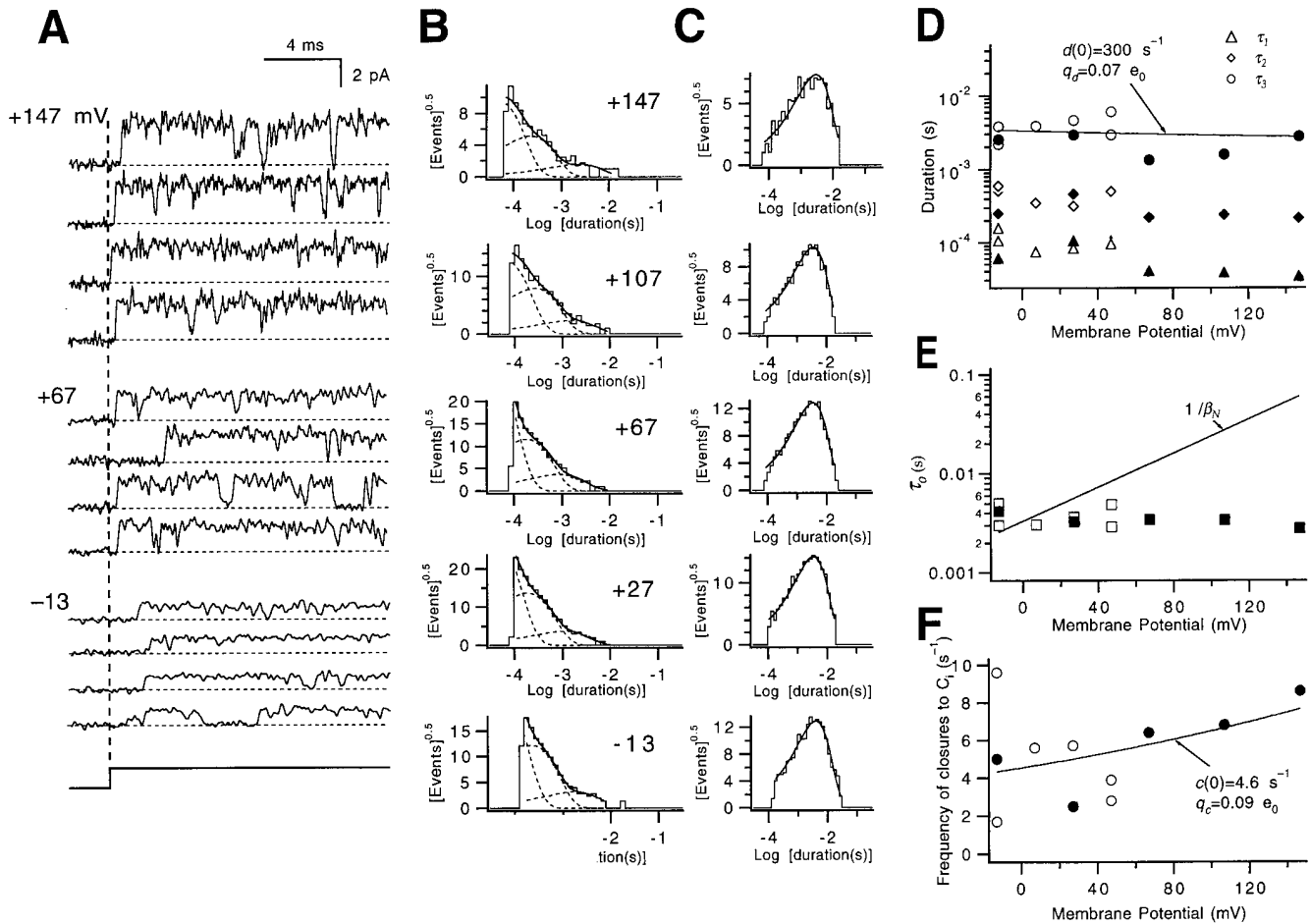


FIGURE 10. Single channel activity at depolarized voltages. (A) Traces of single channel currents elicited by voltage pulses from -93 mV to different test voltages. The beginning of the voltage pulse is indicated by the vertical dashed line. Patches w265 and w276. (B) Closed dwell-time histograms from depolarizations in 40 -mV increments between -13 and $+147$ mV. The histograms were fitted to the sum of three exponentials; dashed curves correspond to each of the fitted exponential components. The number of events in each histogram is ≥ 605 . (C) The open dwell-time histograms at the same voltages were well fitted by a single exponential. (D) The time constants (τ_1 , τ_2 , and τ_3) of the fast, intermediate, and slow exponential components of the closed-time histograms have nearly voltage-independent values near 0.1 , 0.3 , and 2 ms. The τ_3 values were fitted to an exponential (solid line) to estimate the rate d from C_{iN} to the open state. Data points reflect pooled results from several patches. Time constant values from the fits of the histograms shown in B are indicated by the filled symbols. (E) The time constants τ_0 of the single exponentials fitted to the open times display little voltage dependence. Also, the large discrepancy between τ_0 and the reciprocal of the channel closing rate β_N (solid line) indicates that nearly all of the closures at depolarized voltages are to states that are not in the activation path. The τ_0 values from the fits of the histograms shown in C are indicated by the filled symbols. (F) An estimate for the rate c from the open state to C_{iN} was derived by fitting an exponential (solid curve) to estimates of the frequency of C_i closures, corresponding to the τ_3 component in the closed dwell-time distributions. Frequency estimates were obtained from the measured channel open times normalized by the relative contribution of the C_i closures to the total number of measured closures. Values obtained from the histograms in B and C are indicated by the filled symbols. For the closed dwell-time histograms shown in B, the relative amplitudes A_1 , A_2 , and A_3 of the fast, intermediate, and slow exponential components are as follows: at -13 mV, 0.74 , 0.24 , and 0.02 ; at $+27$ mV, 0.83 , 0.16 , and 0.01 ; at $+67$ mV, 0.79 , 0.20 , 0.02 ; at $+107$ mV, 0.83 , 0.16 , and 0.01 ; and at $+147$ mV, 0.85 , 0.14 , and 0.01 .

but also from closed states in the activation path. This property for C_i is required by the fact that C_i contributes to occasionally observed long first latencies to channel opening at depolarized voltages.

An instance in which the channel enters into a long-lived closed state before it opens is evident in the second trace at $+67$ mV in Fig. 10 A. Entries into long-lived closed states before first opening are also apparent in the shape of the cumulative first latency histogram

(Fig. 11 A), which displays a gradual rise superimposed on the dominant faster component. The same slow component was also usually observed in the time course of macroscopic ionic currents at high depolarized voltages ($V \geq +67$ mV; Fig. 4 A). While a single-exponential fit may account for the time course for even a complex gating scheme depending on the way that the fitting is performed, the observed deviation from a single-exponential time course in the final approach of the current

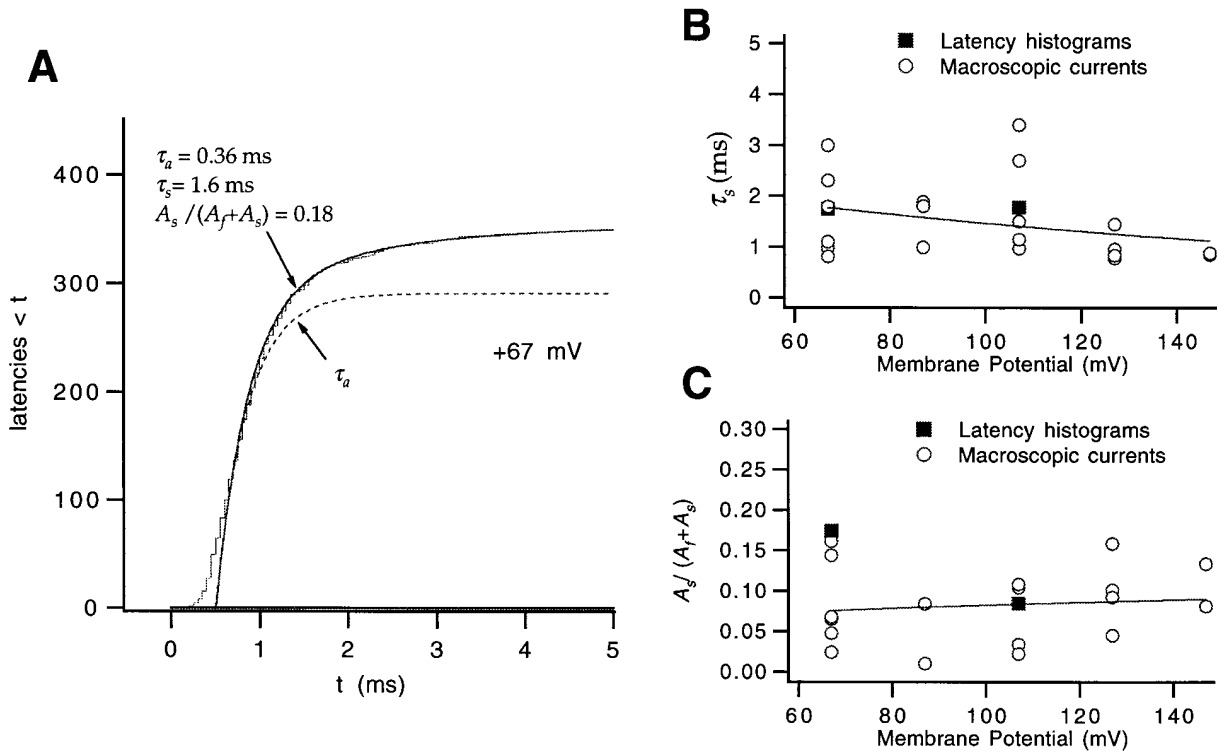


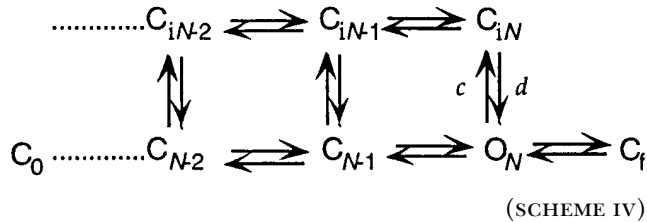
FIGURE 11. C_1 states can be entered from closed states in the activation path. (A) The upper half of the cumulative first latency histogram at +67 mV was fitted to the sum of two exponentials (Eq. 6; *solid curve*), yielding the indicated τ_a , τ_s , and relative A_s values. The dashed curve reflects just the fast component in Eq. 6. The difference in the amplitude of the two curves reflects A_s . Patch w265. (B) The time constants τ_s obtained in the fits of Eq. 6 to first latency distributions (■) and macroscopic ionic currents (○) at $V \geq +67$ mV have values of 1–3 ms. Only two of the single channel experiments had enough traces that a slow component could be convincingly discerned in the latency histogram. However, 21 of 28 relatively smooth macroscopic ionic current time courses at $V \geq +67$ mV (measured in seven patches) displayed an unambiguous slow component. The τ_s values were fitted to single exponential (*solid curve*). The derived charge estimate $q = -0.14 e_0$ indicates that the time constant of the slow component is nearly voltage independent. (C) The relative magnitude of the slow exponential component $A_s / (A_f + A_s)$ is also nearly voltage independent. These values were fitted to an exponential, yielding $q = 0.07 e_0$.

in our fits is good evidence that individual channels are traversing different rate-limiting steps to opening. The observed two components in our time courses apparently are not, however, due to differences in the initial conditions for different channels, because the size of the slow component in the macroscopic current does not change with a very hyperpolarizing prepulse to -143 mV (in three patches; data not shown); this prepulse is expected to preload virtually all channels into the very first closed state. The slow component is also probably not due to modal gating, as it was found in one single channel patch recording that there was no apparent pulse–pulse correlation in the appearance of long first latency. Instead, we take the presence of two components in the final approach of the ionic current to imply that there are two pathways to channel opening; that is, a fraction of channels pass through closed states in a slow path that is distinct from the main activation path.

In fits of two single-channel first latency histograms at $V \geq +67$ mV to the sum of two exponentials (Eq. 6), the fitted slow exponential had time constant τ_s values

of 1.6 and 1.8 ms (Fig. 11, A and B), similar to the 1.9 ± 0.5 -ms mean duration of the τ_3 component in the closed dwell-time histograms at the same voltages ($n = 3$; Fig. 10 D). Fits of 21 macroscopic ionic current time courses to Eq. 6 yielded $\tau_s = 1.5 \pm 2$ ms, also similar to τ_3 . (The time course of the slow component in the macroscopic ionic current can be compared with τ_3 because backward rates at high voltages are negligible, making the ionic current have essentially the same time course as the cumulative first latency histogram; Hoshi et al., 1994.) We take the similarity in the latency time constant and τ_3 to imply that the long latencies to opening reflect sojourns in the same family of states as the C_1 closures that follow the first opening, except these sojourns in C_1 are made from closed states in the activation path. The experiments of Hoshi et al. (1994) were not able to discriminate transitions into C_1 before opening because their single channel measurements were not made at sufficiently high voltages; at lower voltages, the kinetics of the transitions through this secondary activation path are not substantially slower than the kinetics of the main activation path.

The slow component accounts for on average $\sim 10\%$ of the total current relaxation (Fig. 11 C), implying that an opening channel has a 10% chance of entering one of a family of C_i states from closed states in the activation path before opening. For example, in the following scheme,



the opening channel might move from the resting state C_0 into C_{N-1} , and then into C_{iN-1} and C_{iN} , before reaching the open state O_N . From which particular set of closed states the channel can enter the C_i states remains unclear. Scheme IV does not include transitions between C_{iN} and C_f , because we prefer a simple model for these states.

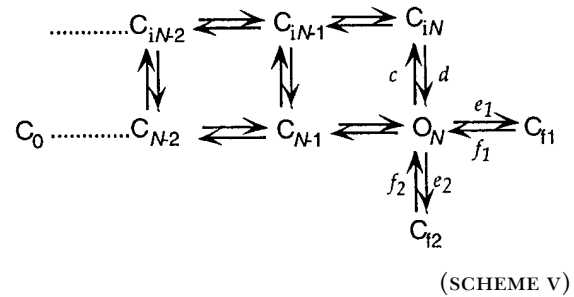
If it is assumed that most of the C_i closures observed at equilibrium at depolarized voltages correspond to sojourns in the state C_{iN} , which is entered directly from the open state, we can use the closed and open dwell-time histograms to assign estimates for the rates c and d of this transition. The values of the time constants fitted to the C_i closures at different voltages give an estimate for the rate d from C_{iN} to the open state ($d(0) = 300 \text{ s}^{-1}$ and $q_d = 0.07 e_0$; Fig. 11 D). The open times and amplitude of the C_i closed time component (Fig. 10 F) give estimates for the rate c from the open state into C_{iN} ($c(0) = 5 \text{ s}^{-1}$ and $q_c = 0.09 e_0$). This estimate for c is an upper limit, if some of the C_i closures observed under equilibrium conditions reflect sojourns in states entered from closed states in the activation path.

Evidence for C_{f1} and C_{f2}

We next evaluate the transitions that correspond to the two rapid components of the closed-time histograms in Fig. 10 B. Since Hoshi et al. (1994) have shown that many of the rapid closures at depolarized voltages are to states that are not in the activation path, our starting hypothesis will be that the two rapid components correspond to two different such states: C_{f1} and C_{f2} . The alternate possibility is that one of the components corresponds to closures in the activation path (e.g., to the last closed state C_{N-1}). We can address this second possibility by comparing the measured channel open times and the reciprocal of our estimated channel closing rate β_N (Fig. 10 E). At the most depolarized voltage where currents were measured (+147 mV), the measured channel open time (3 ms) is 60 times shorter than the expected value of $1/\beta_N = 180 \text{ ms}$ at that voltage. (Were we to correct the open time for missed brief

closures, the discrepancy with $1/\beta_N$ would be even larger.) This large difference implies that virtually all of the measured closures at this voltage reflect closures to states that are not in the activation path. Since the two rapid components of the closed time histograms at +147 mV comprise 73 and 25% of the total measured closures, both very much larger than the $\sim 2\%$ component expected for closures to C_{N-1} , we take both components to reflect closures to states C_{f1} and C_{f2} not in the activation path.

While there are a number of different ways to model these two states, we suggest that C_{f1} and C_{f2} are states into which the open channel closes directly:



We cannot easily rule out alternative models (e.g., having channels in O_N close first into C_{f2} and then into C_{f1}), but we choose Scheme V because of its simplicity.

Since the rapid closures in the single channel recordings are not well resolved, the parameter values derived from exponential fits to the histograms do not yield quantitatively reliable estimates of the rates associated with the transitions to C_{f1} and C_{f2} . We nevertheless obtain rough estimates of these rates by using various strategies.

Estimating Rates for the Transition to C_{f1}

If the transition to either C_{f1} or C_{f2} carries any amount of charge, the rates for this transition can be estimated from the relaxation of macroscopic ionic currents that are elicited by a double pulse protocol. To achieve test currents that predominately reflect the transition to C_{f1} or C_{f2} , prepulses are required that are large enough that virtually no channels reside in states in the activation path at the end of the prepulse. A comparison of the measured channel open times and the reciprocal of the closing rate β_N in Fig. 10 E indicates that at voltages $\geq +7 \text{ mV}$, open times are approximately the same or shorter than $1/\beta_N$; this would imply that much of the test current relaxation after prepulses above +7 mV reflects transitions to states outside the activation path.

Fig. 12 A illustrates an experiment in which we apply voltage steps from +7 to +127 mV, and also from +47 to +147 mV. These voltage jumps elicited small current relaxations with activation time constants of $\tau_r = 230$ and $180 \mu\text{s}$. The time course of the current relaxation at +147 mV ($\tau_r = 180 \mu\text{s}$) is threefold slower than the

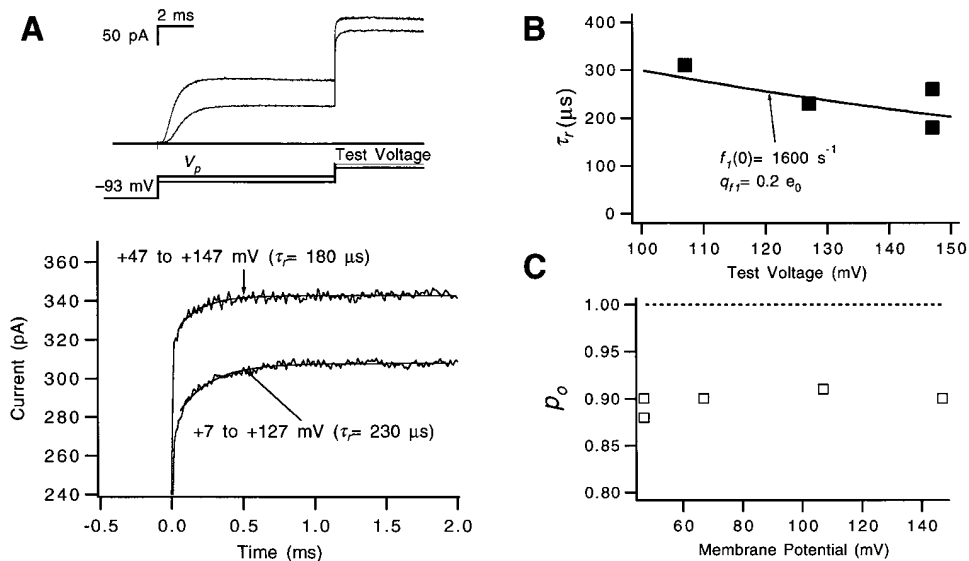


FIGURE 12. Characterization of the transitions to C_{f1} and C_{f2} . (A, top) Macroscopic ionic currents elicited by voltage steps between pairs of depolarized voltages. The smaller current (at both the prepulse and test voltages) reflects a voltage step from +7 to +127 mV, and the larger current reflects a voltage step from +47 to +147 mV. Data were filtered at 15 kHz. Patch w447. (bottom) The same traces are expanded to show just the current relaxation during the test pulse; zero time is the start of the test pulse. The current relaxations are fitted to a single exponential to estimate the time constant τ_r (solid curves). At +127 and +147 mV, the time constants are $\tau_r = 230$ and $180 \mu\text{s}$, respectively, and the amplitudes of the fitted exponentials

are -32 and -21 pA. These amplitudes can be compared with the size of the rest of the test current (278 and 323 pA, respectively) to yield estimates of the change in P_o induced by these voltage steps (10 and 6%). (B) The rate f_1 from C_{f1} to the open state was estimated by fitting an exponential (solid curve) to the τ_r values (■) taken from the current relaxations measured in the experiment in A and from similar measurements made in one other patch. (C) Estimates of absolute P_o at voltages between +47 and +147 mV were derived from the mean measured channel closed and open dwell times in the equilibrium single channel activity. The data points reflect measurements made in four patches. Absolute P_o apparently saturates near 0.9.

fast reactivation time constant that corresponds to the last transition in the activation path (Fig. 5 D); this indicates that the observed current must reflect a transition that is distinct from the last activation transition. The observed relaxation also cannot reflect the transition to C_{iN} . Given the estimates for c and d assigned above, the transition to C_{iN} would contribute to a change in open probability $\Delta P_o \ll 1\%$ during these voltage jumps, but the amplitudes of the relaxations correspond to $\Delta P_o \geq 6\%$ (see legend to Fig. 12). Thus, these relaxations almost certainly reflect transitions to C_{f1} or C_{f2} , and we assign them to C_{f1} . Since these currents are recorded at depolarized voltages, we assume that the current time course mostly reflects the rate f_1 from C_{f1} to the open state, yielding estimates of $f_1(0) = 1,600 \text{ s}^{-1}$ and $q_{f1} = 0.2 e_0$ (Fig. 12 B).

The value of the rate constant e_1 for the entry into C_{f1} can be determined using the amplitude of the current relaxation in the voltage jump experiment in Fig. 12 A. The 10% change in relative P_o induced by the voltage jump from +7 to +127 mV, together with the value for f_1 derived above, gives $e_1 = 190 \text{ s}^{-1}$ at +7 mV (assuming that the transition to C_{f1} is saturated at +127 mV). We assume that this transition is voltage independent.

The current relaxations in Fig. 12 A verify one feature of data presented earlier in this paper. In the voltage dependence of channel opening for *Shaker* (Fig. 1), P_o rises steeply to $\sim 80\%$ of its maximal value, but displays a slow upward drift at higher voltages. The pres-

ence of the gradual rise, however, has been reported to be dependent on the method by which P_o is measured (Zagotta et al., 1994a). The 12% change in relative P_o that we estimate to occur between +7 and +67 mV using the tail-current method for estimating relative P_o (described in the legend of Fig. 1) is, notably, similar to the 10% change in relative P_o induced by the voltage jump from +7 to +127 mV. In our modeling paper (Schoppa and Sigworth, 1998b), we will use the shape of the P_o -V relation at depolarized voltages to help constrain the total charge associated with the transition to C_{f1} .

Estimating Rates of the Transition to C_{f2}

The relaxations of the macroscopic currents in Fig. 12 A that correspond to $C_{f1} \rightarrow O$ have similar time-constant values as the intermediate duration τ_2 component of the single-channel closed dwell-time histograms at similar voltages (Fig. 10 D); at $V > +100$ mV, τ_2 is between 200 and 300 μs . If the transition from C_{f1} corresponds roughly to the intermediate duration closures in the dwell-time histograms, the transition from C_{f2} must correspond to the very rapid 40–100 μs closures. These closures are poorly resolved, but the short apparent time constant implies that the rate f_2 from C_{f2} to the open state is very rapid (near 10^4 s^{-1}). Information about this transition can also be obtained from estimates of absolute P_o , which can be derived from the mean open and closed times in the single channel mea-

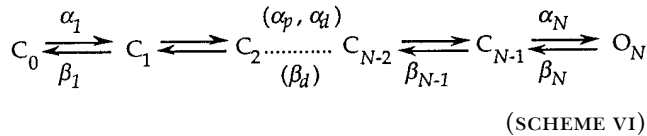
surements (Fig. 12 C). From measurements obtained at voltages as large as +147 mV, the derived absolute P_o values apparently saturate near 0.9. The fact that P_o at very high voltages saturates at a value less than unity implies that the transition to C_{i2} is nearly voltage independent (giving $q_{e2} + q_{f2} \approx 0.0$). A saturating value of $P_o = 0.9$ implies a ratio of the two rates e_2/f_2 near 0.1, giving $e_2 \approx 10^3 \text{ s}^{-1}$.

DISCUSSION

In this and the following two papers (Schoppa and Sigworth, 1998a, 1998b), we characterize activation gating for the normally activating *Shaker* channel (WT) and a mutant version of the channel to arrive at a relatively well-constrained activation gating model. In this first paper, we have undertaken a detailed analysis of the kinetics of WT's macroscopic ionic and gating currents and single channel currents in an effort to obtain estimates of several rate constants. Previous efforts at characterizing *Shaker's* activation gating process exploited experimental strategies that were similar to ours in order to isolate particular activation gating transitions (Hoshi et al., 1994; Zagotta et al., 1994a; Bezanilla et al., 1994a). However, we have gained new insights by analyzing the current time courses in novel ways and by extending the voltage range of the current measurements.

Estimates of Forward and Backward Rates for Transitions in the Activation Path

We have assumed that activation gating is described by a Markov process with transitions between discrete states separated by large energy barriers. Fits of exponentials to selected ionic and gating current time courses at extreme voltages yielded estimates of the rate constants depicted here.



For the forward rates, we have obtained estimates of the first forward rate α_1 , the limiting rate at large positive potentials α_p , the final opening rate α_N , and an estimate of the partial charge $q_{\alpha d}$ that determines the voltage dependence of forward rates of intermediate steps. For backward rates, we have obtained estimates of the first and last two backward rates (β_1 , β_{N-1} , and β_N), and an estimate of the backward rates of intermediate steps β_d . The values obtained are given in Table I. We have also extended on the work of Hoshi et al. (1994) by characterizing the transitions to several closed states that are not normally traversed before the channel opens. Hoshi et al. (1994) showed that there were at

TABLE I

<i>Estimates of Rate Constants for Transitions in the Activation Path</i>	
Rate (0 mV)	Partial charge
$\alpha_1(0) = 1200 \text{ s}^{-1}$	$q\alpha_1 = 0.36 e_0$
$\alpha_p(0) = 2100 \text{ s}^{-1}$	$q\alpha_p = 0.17 e_0$
$\alpha_N(0) = 7000 \text{ s}^{-1}$	$q\alpha_N = 0.18 e_0$
—	$q\alpha_d = 0.25 e_0$
$\beta_1(0) = 190 \text{ s}^{-1}$	$q\beta_1 = -0.53 e_0$
$\beta_N(0) = 150 \text{ s}^{-1}$	$q\beta_N = -0.57 e_0$
$\beta_{N-1}(0) = 320 \text{ s}^{-1}$	$q\beta_{N-1} = -0.30 e_0$
$\beta_d(0) = 540 \text{ s}^{-1}$	$q\beta_d = -0.24 e_0$

least two such states C_i and C_j ; from an analysis of single channel data, we have shown that there are at least four such states. These results are summarized by Scheme V above and the list of rate estimates in Table II.

It should be emphasized that the parameters $q_{\alpha d}$, $q_{\beta d}$, and $\beta_d(0)$ that we ascribe to intermediate transitions should be taken as quite rough approximations; these are shown in Scheme VI with parentheses. The charge parameters $q_{\alpha d}$ and $q_{\beta d}$ were derived from the delay in the channel opening time course, which reflects the composite properties of many transitions. These parameters are also somewhat difficult to interpret because transitions with the fastest forward rates contribute little to the delay. Thus, these charge parameters are not likely to reflect the partial charges associated with the most rapid transitions. However, the number of rates with partial charges similar to $q_{\alpha d}$ and $q_{\beta d}$ is likely to be quite large. Zagotta et al. (1994b) estimated that a minimum of five transitions are required to account for the delay in the ionic current time course; our own analysis gives a minimum estimate of seven transitions (Schoppa et al., 1998b), implying that at least six transitions contribute significantly to the delay.

Assumptions Used in the Derivation of Rate Constants

The accuracy of these rate estimates has relied on a number of assumptions, besides the assumption of a Markov process. The first of these is that our current measurements were made at sufficiently positive and negative voltages to yield unidirectional transitions, so

TABLE II

<i>Estimate of Rate Constants for Transitions to States Outside of the Activation Path</i>	
Rate (0 mV)	Partial charge
$c \leq 5 \text{ s}^{-1}$	$qc = 0.09 e_0$
$d = 300 \text{ s}^{-1}$	$qd = 0.07 e_0$
$e \approx 200 \text{ s}^{-1}$	$qe \approx 0$
$f_1 = 1600 \text{ s}^{-1}$	$qf_1 = 0.20 e_0$
$e_2 \approx 10^3 \text{ s}^{-1}$	$qe_2 - qf_2 = 0$
$f_2 \approx 10^4 \text{ s}^{-1}$	

that our current measurements reflect only a single microscopic rate constant. All but one of the forward rates were estimated from currents measured at $V \geq +67$ mV, which is 80 mV higher than where the Q - V relation saturates, and all backward rates were estimated from currents measured at $V \leq -93$ mV, where $<8\%$ of the charge movement occurs. While we cannot be certain that transitions are unidirectional at these voltages, our current measurements were made at more extreme voltages than those that have been published previously. Thus, for example, in the estimate of the channel closing rate β_N , our estimates are likely to be more reliable than those that have been reported previously.

The forward rate α_1 of the first transition was estimated from current measurements made at voltages between -13 and $+67$ mV. The reason for concern about voltage ranges for this estimate is the following. Whereas the equilibrium P_o - V and Q - V relations appear to saturate near 0 mV (Fig. 1), previous models for *Shaker*'s gating (Bezanilla et al., 1994; Zagotta et al., 1994b) have included at least one transition that has a relatively large backward rate at this voltage; the channel nevertheless opens due to the driving action of a later forward-biased transition. Thus, for example, non-negligible backward rates at voltages near 0 mV will yield an estimate for α_1 from the final approach of the ionic current that is smaller than its actual value.

A second assumption that we have made for simplicity is that activation gating follows a linear sequence of transitions as in Scheme VI. Many of the models that have been used to describe the activation gating process for *Shaker* channels, however, are branched models that reflect the tetrameric structure of the channels (McCormick et al., 1994; Zagotta et al., 1994b); we also will propose branched models in a subsequent paper. The estimates for rate constants given here are likely to be valid for such branched models. Many of our rate estimates rely on fits of exponentials to macroscopic ionic current time courses yielding a time constant τ_a and a delay parameter δ_a . As we have shown in the simulations of branched models in Fig. 2, *C* and *D*, the rates of rate-limiting steps are estimated without large errors by this approach.

In this paper, we have considered evidence that activation gating for *Shaker* deviates from a sequential model in that there are three closed states (C_{iN} , C_{f1} , and C_{f2}) that the channel enters after the channel opens, and at least one additional closed state C_i that the channel can enter from closed states in the activation path. The transitions to the three states C_{iN} , C_{f1} , and C_{f2} are problematic to our analysis because these transitions could affect the macroscopic tail current and reactivation time courses that yielded our estimates of α_N , β_N , and β_{N-1} . For example, channels undergoing slightly voltage-dependent transitions from the open

state to C_{iN} or C_{f1} could contribute to additional decay components in the tail current (Zagotta et al., 1994a). However, these components are expected to be small due to the transitions' small voltage dependences; also, at hyperpolarized voltages (-193 mV), the rates of the transitions from the open state to C_{iN} and C_{f1} ($c = 3$ s $^{-1}$ and $e_1 = 10^3$ s $^{-1}$) are much smaller than the rate of channel closing into the activation path ($\beta_N(-193) = 11,400$ s $^{-1}$). The additional states C_i entered from closed states in the activation path make a small contribution to the channel activation time course at high voltages, and thus could affect our estimate of the high voltage rate-limiting step α_p ; however, we explicitly account for these transitions by fitting the ionic currents to the sum of two exponentials.

The best evidence that the simplified analysis of the *Shaker*'s gating process in this paper is reasonable comes from comparing the first-pass estimates of various rates obtained here (in Tables I and II) with the results of the modeling in the third paper in this series (Schoppa and Sigworth, 1998b). There, we consider a number of different branched models that are similar to Scheme II. We derive starting rate estimates for the transitions in the models from each of the rate estimates obtained here; the rate values that then yield the best fits of the data are quite similar to these starting estimates, being at most a factor of 2–3 different.

Activation Gating Involves Many Transitions with Small Valences

The characterization of the different activation gating transitions performed in this paper leads to a few general results about the activation gating process. The first is a rough estimate of the average amount of charge associated with each of the transitions. We use here the estimated partial charges (q_{ad} and q_{bd}) for the forward and backward rates, which were derived from the delay in the channel opening time courses. The derived q_{ad} and q_{bd} estimates (0.25 and -0.24 e_0) yield a single transition charge estimate ($q_{ad} - q_{bd}$) of 0.5 e_0 . This estimate of the average amount of charge associated with each transition, in turn, leads to an estimate of the number of gating transitions n . If an activating *Shaker* channel moves a total charge of 13 e_0 (Schoppa et al., 1992; Aggarwal and MacKinnon, 1996; Seoh et al., 1996), our estimate of 0.5 e_0 for the transition charge implies that an opening channel undergoes $n \approx 26$ gating transitions.

The value of 0.5 e_0 for the transition charge may be too small since, as described above, the delay does not provide a good measure of the transitions with the most rapid rates. Indeed, fluctuation analysis of gating currents at depolarized voltages (Sigg et al., 1994b; 1996) suggests that there are some transitions that have

valences near 2. These considerations also imply that the estimate of 26 transitions may be somewhat too large.

Activation Gating Involves at least Three Different Types of Gating Transitions

A second insight that we obtain here is an estimate of the number of different types of gating transitions. This is derived from the partial charges that define the voltage dependences of the different rates. The list in Table I includes $q_{\alpha 1} = 0.36 e_0$, $q_{\alpha N} = 0.18 e_0$, $q_{\beta 1} = -0.53$

e_0 , $q_{\beta N-1} = -0.30 e_0$, and $q_{\beta N} = -0.57 e_0$. From these estimates, two types of transitions can be distinguished by having different partial charges for their forward rates. These correspond to the very first and very last transitions, with charges $q_{\alpha 1}$ and $q_{\alpha N}$. A third transition has a partial charge for its backward rate ($q_{\beta N-1} = -0.30 e_0$) that is different from that for the backward rate of either the first or last transition ($q_{\beta 1} = -0.53 e_0$ and $q_{\beta N} = -0.57 e_0$). These considerations will be important in the discrimination between different models in the third paper in this series (Schoppa and Sigworth, 1998b).

We thank L. Lin for oocyte preparation; E. Moczydlowski and R. MacKinnon for CTx; and R.K. Ayer, W.K. Chandler, K. McCormack, Y. Yang, and W.N. Zagotta for helpful discussions.

This study was supported by National Institutes of Health grant NS-21501 to F.J. Sigworth.

Original version received 3 June 1997 and accepted version received 24 November 1997.

REFERENCES

- Aggarwal, S.K., and R. MacKinnon. 1996. Contribution of the S4 segment to gating charge in the *Shaker* K⁺ channel. *Neuron*. 16: 1169–1177.
- Armstrong, C.M., and F. Bezanilla. 1973. Currents related to the movement of the gating particles of the sodium channels. *Nature*. 242:459–461.
- Bezanilla, F., E. Perozo, D.M. Papazian, and E. Stefani. 1991. Molecular basis of gating charge immobilization in *Shaker* potassium channels. *Science*. 254:679–683.
- Bezanilla, F., E. Perozo, and E. Stefani. 1994. Gating of *Shaker* K⁺ channels: II. The components of gating currents and a model of channel activation. *Biophys. J.* 66:1011–1021.
- Cole, K.S., and J.W. Moore. 1960. Potassium ion current in the squid giant axon: dynamic characteristic. *Biophys. J.* 1:1–14.
- Colquhoun, D., and F.J. Sigworth. 1995. Fitting and statistical analysis of single-channel records. In *Single-Channel Recording*. 2nd ed. B. Sakmann and E. Neher, editors. Plenum Publications, Inc., New York. 483–588.
- Conti, F., and W. Stuhmer. 1989. Quantal charge redistributions accompanying the structural transitions of sodium channels. *Eur. Biophys. J.* 17:53–59.
- Crouzy, S.C., and F.J. Sigworth. 1993. Fluctuations in ion channel gating currents. Analysis of nonstationary shot noise. *Biophys. J.* 64:68–76.
- Guy, H.R., and P. Seetharamulu. 1986. Molecular model of the action potential sodium channel. *Proc. Natl. Acad. Sci. USA*. 83:508–512.
- Hamill, O.P., A. Marty, E. Neher, B. Sakmann, and F.J. Sigworth. 1981. Improved patch-clamp techniques for high-resolution current recording from cells and cell-free membrane patches. *Pflügers Arch. Eur. J. Physiol.* 391:85–100.
- Heginbotham, L., and R. MacKinnon. 1993. Conduction properties of the cloned *Shaker* K⁺ channel. *Biophys. J.* 65:2089–2096.
- Hodgkin, A.L., and A.F. Huxley. 1952a. Currents carried by sodium and potassium ions through the membrane of the giant axon of *Loligo*. *J. Physiol. (Camb.)*. 116:449–472.
- Hodgkin, A.L., and A.F. Huxley. 1952b. A quantitative description of membrane current and its application to conduction and excitation in nerve. *J. Physiol. (Camb.)*. 117:500–544.
- Horn, R., and K. Lange. 1983. Estimating kinetic constants from single channel data. *Biophys. J.* 43:207–223.
- Hoshi, T., W.N. Zagotta, and R.W. Aldrich. 1990. Biophysical and molecular mechanisms of *Shaker* potassium channel inactivation. *Science*. 250:533–538.
- Hoshi, T., W.N. Zagotta, and R.W. Aldrich. 1991. Two types of inactivation in *Shaker* K⁺ channels: effects of alterations in the carboxy-terminal region. *Neuron*. 7:547–556.
- Hoshi, T., W.N. Zagotta, and R.W. Aldrich. 1994. *Shaker* potassium channel gating I: transitions near the open state. *J. Gen. Physiol.* 103:249–278.
- Iverson, L.E., and B. Rudy. 1990. The role of divergent amino and carboxyl domains on the inactivation properties of potassium channels derived from the *Shaker* gene of *Drosophila*. *J. Neurosci.* 10:2903–2916.
- Kamb, A., J. Tseng-Crank, and M.A. Tanouye. 1988. Multiple products of the *Drosophila Shaker* gene may contribute to potassium channel diversity. *Neuron*. 1:421–430.
- Kavanaugh, M.P., R.S. Hurst, J. Yakel, M.D. Varnum, J.P. Adelman, and R.A. North. 1992. Multiple subunits of a voltage-dependent potassium channel contribute to the binding site for tetraethylammonium. *Neuron*. 8:493–497.
- Keynes, R.D., and E. Rojas. 1974. Kinetics and steady state properties of the charged system controlling sodium conductance in the squid giant axon. *J. Physiol. (Camb.)*. 233:393–434.
- Larsson, H.P., O.S. Baker, D.S. Dhillon, and E.Y. Isacoff. 1996. Transmembrane movement of the *Shaker* K⁺ channel S4. *Neuron*. 16:387–397.
- Li, M., N. Unwin, K.A. Stauffer, Y.N. Jan, and L.Y. Jan. 1994. Images of purified *Shaker* potassium channels. *Curr. Biol.* 4:110–115.
- Liman, E.R., P. Hess, F. Weaver, and G. Koren. 1991. Voltage-sensing residues in the S4 region of a mammalian K⁺ channel. *Nature*. 353:752–756.
- Logothetis, D.E., S. Movahedi, C. Satler, K. Lindpaintner, and B. Nadal-Ginard. 1992. Incremental reductions of positive charge within the S4 region of a voltage-gated K⁺ channel result in corresponding decreases in gating charge. *Neuron*. 8:531–540.
- Lopez, G.A., Y.N. Jan, and L.Y. Jan. 1991. Hydrophobic substitution mutations in the S4 sequence alter voltage-dependent gating in

- Shaker* K⁺ channels. *Neuron*. 7:327–336.
- Lopez-Barneo, J., T. Hoshi, S.H. Heinemann, and R.W. Aldrich. 1993. Effects of external cations and mutations in the pore region of K⁺ channels. *Receptors Channels*. 1:61–72.
- Lucchesi, K., A. Ravindran, H. Young, and E. Moczydlowski. 1989. Analysis of the blocking activity of charybdotoxin homologs and iodinated derivatives against Ca²⁺-activated K⁺ channels. *J. Membr. Biol.* 109:269–281.
- MacKinnon, R. 1991. Determination of the subunit stoichiometry of a voltage-activated potassium channel. *Nature*. 350:232–235.
- Mannuzzu, L.M., M.M. Moronne, and E.Y. Isacoff. 1996. Direct physical measure of conformational rearrangement underlying potassium channel gating. *Science*. 271:213–216.
- McCormack, K., W.J. Joiner, and S.H. Heinemann. 1994. A characterization of the activating structural rearrangements in voltage-dependent *Shaker* K⁺ channels. *Neuron*. 12:301–315.
- McCormack, K., M.A. Tanouye, L.E. Iverson, J.W. Lin, M. Ramaswami, T. McCormack, J.T. Campanelli, M.K. Mathew, and B. Rudy. 1991. A role for hydrophobic residues in the voltage-dependent gating of *Shaker* K⁺ channels. *Proc. Natl. Acad. Sci. USA*. 88:2931–2935.
- McManus, O.B., and K.L. Magleby. 1988. Kinetic states and modes of single large-conductance calcium-activated potassium channels in cultured rat skeletal muscle. *J. Physiol. (Camb.)*. 402:79–120.
- Neher, E. 1992. Correction for liquid junction potentials in patch clamp experiments. *Methods Enzymol.* 207:123–131.
- Noda, M., T. Ikeda, H. Suzuki, H. Takeshima, T. Takahashi, M. Kuno, and S. Numa. 1986. Expression of functional sodium channels from cloned cDNA. *Nature*. 322:826–828.
- Noda, M., S. Shimuzi, T. Tanabe, T. Takai, T. Kayano, T. Ikeda, H. Takahashi, H. Nakayama, Y. Kanaoka, N. Minamino, et al. 1984. Primary structure of *Electrophorus electricus* sodium channel deduced from cDNA sequence. *Nature*. 312:121–125.
- Papazian, D.M., L.C. Timpe, Y.N. Jan, and L.Y. Jan. 1991. Alteration of voltage-dependence of *Shaker* potassium channel by mutations in the S4 sequence. *Nature*. 349:305–310.
- Perozo, E., D.M. Papazian, R.E. Weiss, L. Toro, E. Stefani, and F. Bezanilla. 1994. S4 mutations alter gating currents of *Shaker* K⁺ channels. *Biophys. J.* 66:345–354.
- Schneider, M.F., and W.K. Chandler. 1973. Voltage-dependent charge movement in skeletal muscle: a possible step in excitation–contraction coupling. *Nature*. 242:244–246.
- Schoppa, N.E., K. McCormack, M.A. Tanouye, and F.J. Sigworth. 1992. Estimate of the total gating charge in *Shaker* potassium channels. *Science*. 255:1712–1715.
- Schoppa, N.E., and F.J. Sigworth. 1998a. Activation of *Shaker* potassium channels. II. Kinetics of the V2 mutant channel. *J. Gen. Physiol.* 111:295–311.
- Schoppa, N.E., and F.J. Sigworth. 1998b. Activation of *Shaker* potassium channels. III. An activation gating model for wild-type and V2 mutant channels. *J. Gen. Physiol.* 111:313–342.
- Seoh, S.-A., D. Sigg, and F. Bezanilla. 1996. Voltage-sensing residues in the S2 and S4 segments of the *Shaker* K⁺ channel. *Neuron*. 16:1159–1167.
- Sigg, D., F. Bezanilla, and E. Stefani. 1994a. Slowing of deactivation kinetics in *Shaker* B as seen in macropatch recordings of gating and ionic currents. *Biophys. J.* 66:A439. (Abstr.)
- Sigg, D., E. Stefani, and F. Bezanilla. 1994b. Gating current noise produced by elementary transitions in *Shaker* potassium channels. *Science*. 264:578–582.
- Sigg, D., E. Stefani, H. Qian, and F. Bezanilla. 1996. Quasi-equilibrium noise analysis of *Shaker* K⁺ channel gating currents. *Biophys. J.* 70:144a. (Abstr.)
- Sigworth, F.J. 1983. An Example of analysis. In *Single-Channel Recording*. 1st ed. B. Sakmann and E. Neher, editors. Plenum Publications, Inc., New York. 301–322.
- Sigworth, F.J. 1994. Voltage gating of ion channels. *Q. Rev. Biophys.* 27:1–40.
- Sigworth, F.J., and S.M. Sine. 1987. Data transformations for improved display and fitting of single-channel dwell-time histograms. *Biophys. J.* 52:1047–1052.
- Stefani, E., L. Toro, E. Perozo, and F. Bezanilla. 1994. Gating of *Shaker* K⁺ channels. I. Ionic and gating currents. *Biophys. J.* 66:996–1010.
- Stühmer, W., F. Conti, M. Stocker, O. Pongs, and S.H. Heinemann. 1991. Gating currents of inactivating and non-inactivating potassium channels expressed in *Xenopus* oocytes. *Pflügers Arch. Eur. J. Physiol.* 418:423–429.
- Stühmer, W., F. Conti, H. Suzuki, X.D. Wang, M. Noda, N. Yahagi, H. Kubo, and S. Numa. 1989. Structural parts involved in activation and inactivation of the sodium channel. *Nature*. 339:597–603.
- Tanabe, T., H. Takeshima, A. Mikami, V. Flockerzi, H. Takahashi, K. Kangawa, M. Kojima, H. Matsuo, T. Hirose, and S. Numa. 1987. Primary structure of the receptor for calcium channel blockers from skeletal muscle. *Nature*. 328:313–318.
- Tempel, B.L., D.M. Papazian, T.L. Schwarz, Y.N. Jan, and L.Y. Jan. 1987. Sequence of a probable potassium channel component encoded at the *Shaker* locus of *Drosophila*. *Science*. 237:770–775.
- Tytgat, J., and P. Hess. 1992. Evidence for cooperative interactions in potassium channel gating. *Nature*. 359:420–423.
- Yang, N., A.L.J. George, and R. Horn. 1996. Molecular basis of charge movement in voltage-gated sodium channels. *Neuron*. 16:113–122.
- Yang, N., and R. Horn. 1995. Evidence for voltage-dependent S4 movement in sodium channels. *Neuron*. 15:213–218.
- Zagotta, W.N., T. Hoshi, and R.W. Aldrich. 1994b. *Shaker* potassium channel gating. III. Evaluation of kinetic models for activation. *J. Gen. Physiol.* 103:321–362.
- Zagotta, W.N., T. Hoshi, J. Dittman, and R.W. Aldrich. 1994a. *Shaker* potassium channel gating. II. Transitions in the activation pathway. *J. Gen. Physiol.* 103:279–319.